CHAPTER III
RESULTS AND DISCUSSION

3.1 Dynamic Mechanical Properties

Unreduced storage moduli and tanδ of PMMA M_w = 350000 $gmol^{-1}$, PMMA M_w = 75000 $gmol^{-1}$, SAN 75:25, and PMMA/SAN 30/70 blends plotted as functions of frequency and temperature are shown in Figures 3.1, 3.2, 3.3, and 3.4 respectively. The temperature was varied from 60 °C to 190 °C covering the glassy regime below T_g to the terminal regime well above T_g . The frequency was varied from 0.01 rad/s to 100 rad/s, covering 5 decades of frequency. The data were taken in the frequency/temperature scan mode with a soak time of 600 seconds between each frequency scan. We were careful in applying a minimum compressive force on the samples so that they were close to the ideal torsional deformation.

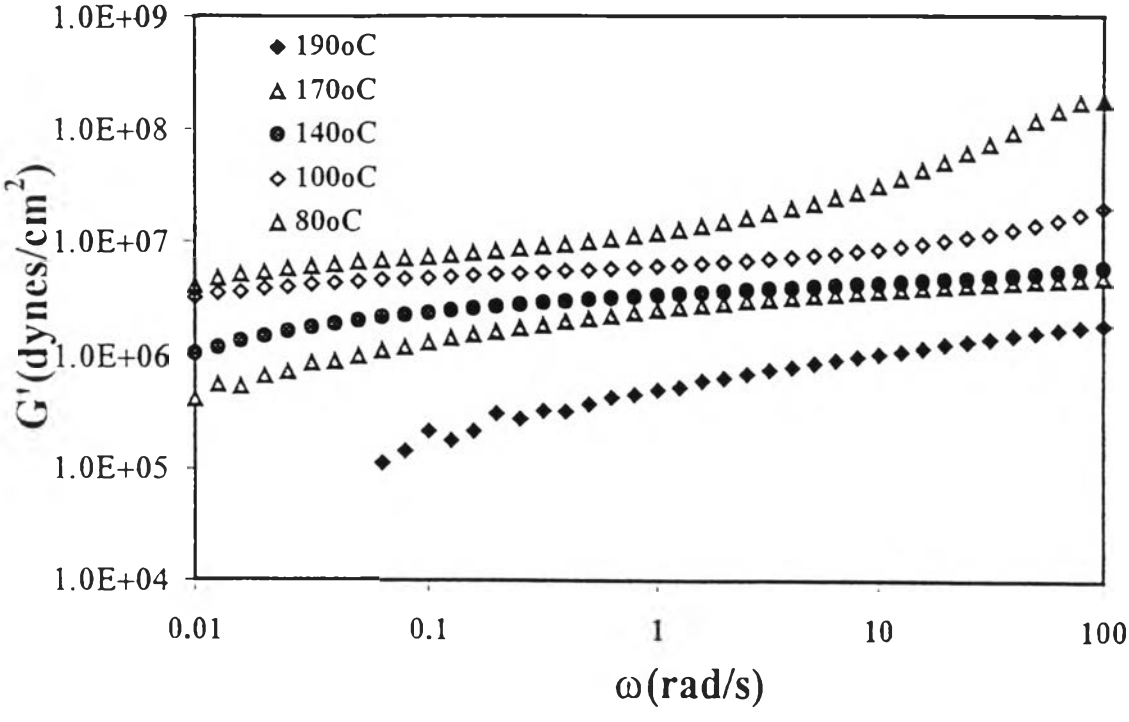

Figure 3.1 (a) Unreduced storage moduli of PMMA M_W = 350000 gmol^{-1} at various temperatures above and below T_g, with % strain of 0.25.

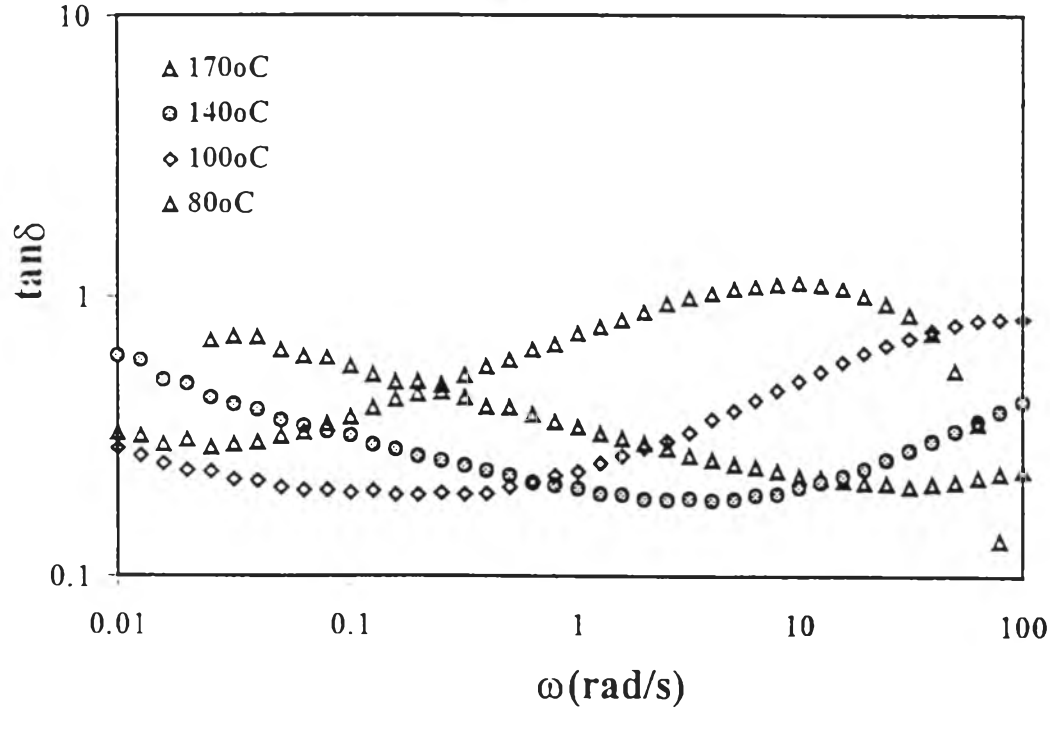

Figure 3.1 (b) Unreduced tanδ of PMMA M_W = 350000 gmol^{-1} at various temperatures above and below T_g, with % strain of 0.25.

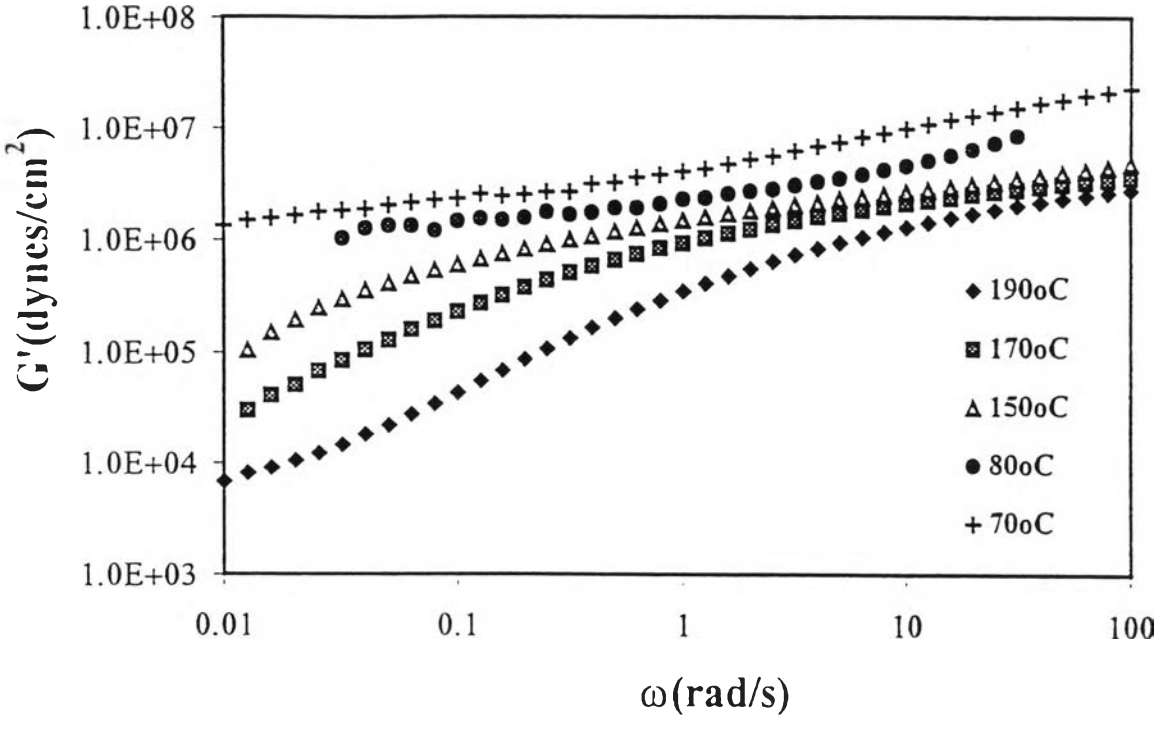

Figure 3.2 (a) Unreduced storage moduli of PMMA M_W = 75000 gmol^{-1} at various temperatures above and below T_g, with % strain of 0.25.

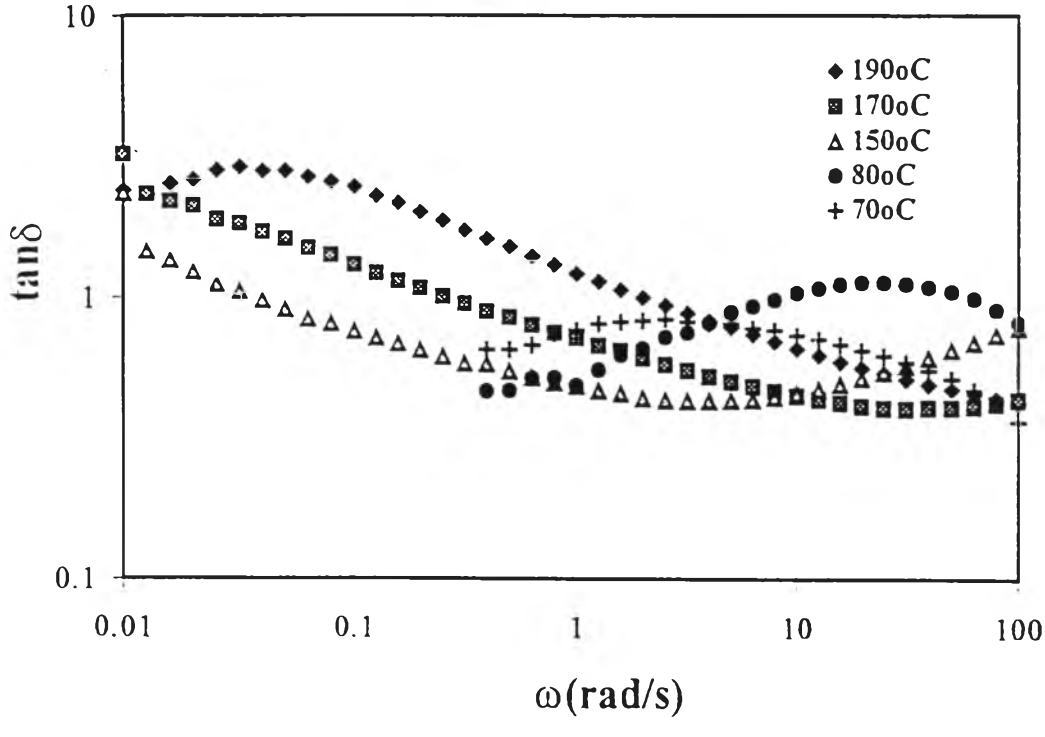

Figure 3.2 (b) Unreduced tanδ of PMMA M_W = 75000 gmol^{-1} at various temperatures above and below T_g, with % strain of 0.25.

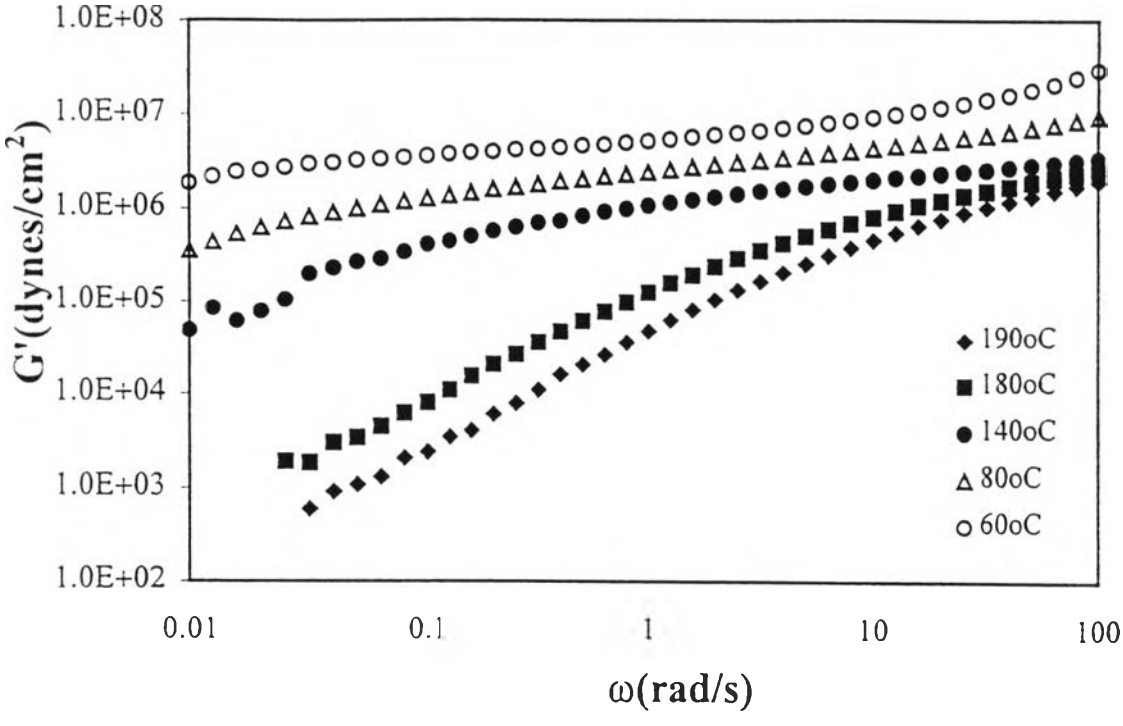

Figure 3.3 (a) Unreduced storage moduli of SAN75:25 at various temperatures above and below T_g, with %strain of 0.25.

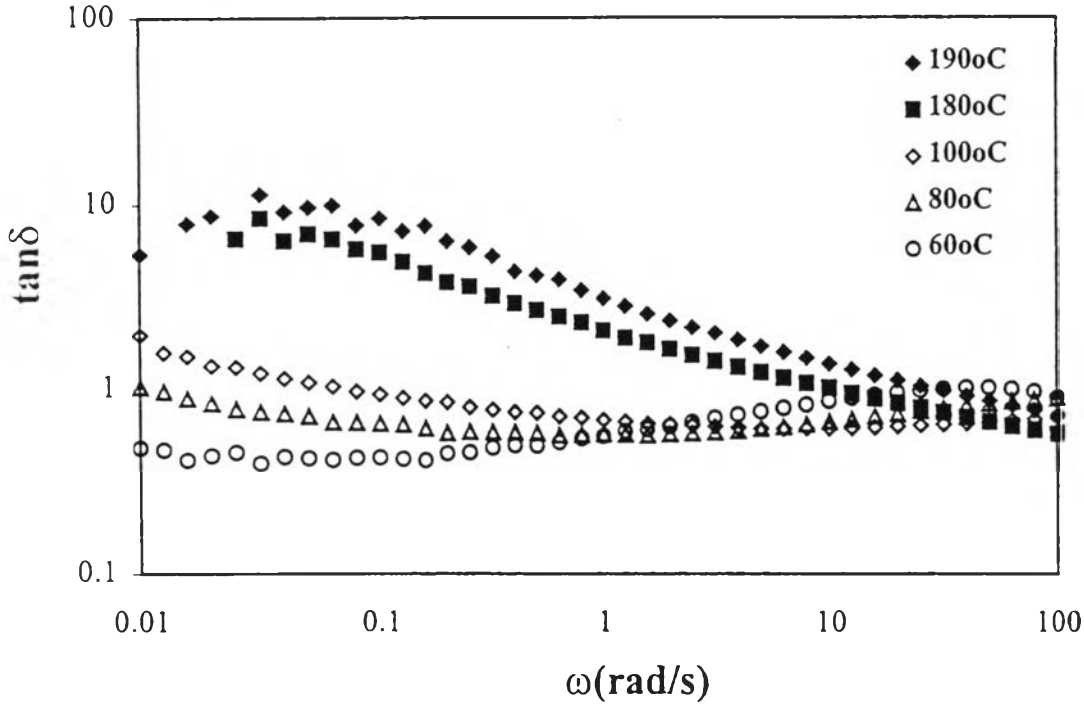

Figure 3.3 (b) Unreduced tanδ of SAN75:25 at various temperatures above and below T_g, with %strain of 0.25.

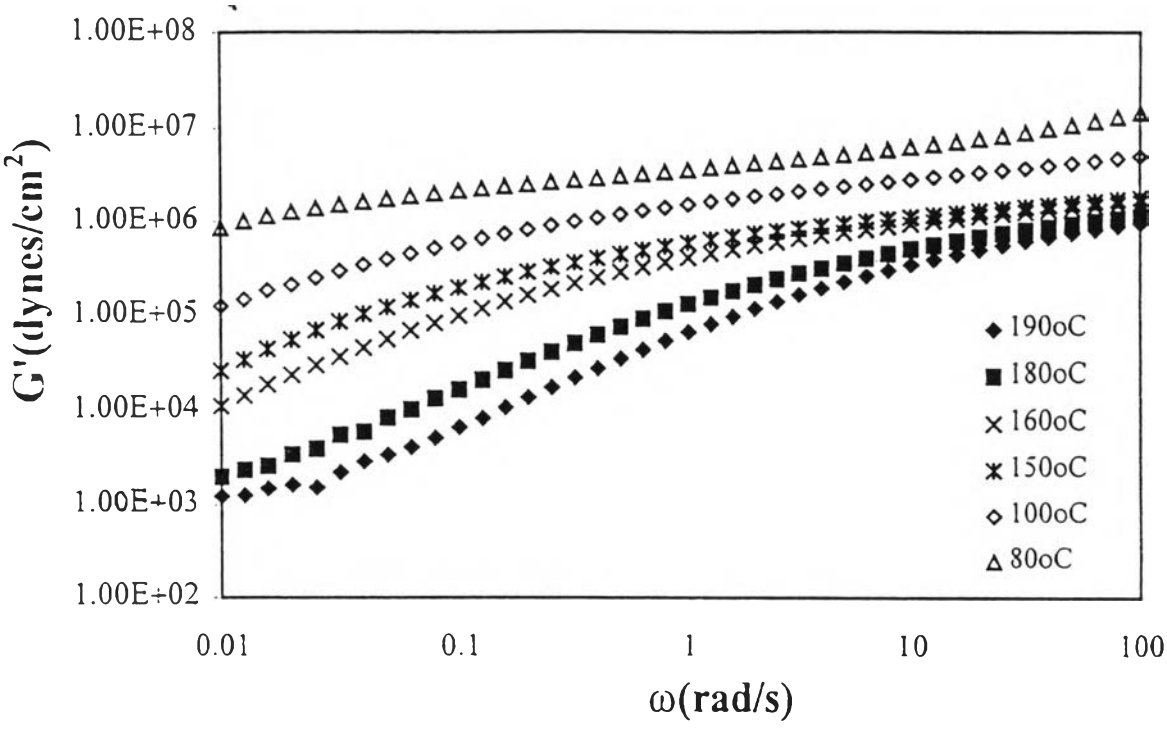

Figure 3.4 (a) Unreduced storage moduli of PMMA/SAN 30/70 blends at various temperatures above and below T_g, with %strain of 0.70.

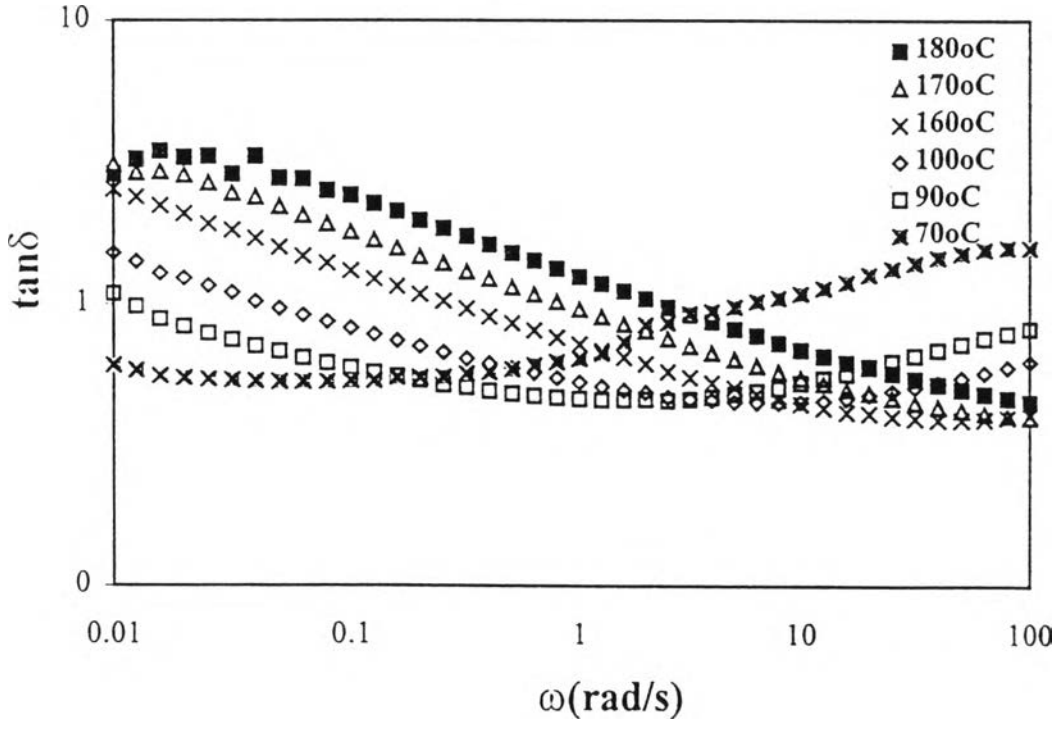

Figure 3.4 (b) Unreduced tanδ of PMMA/SAN 30/70 blends at various temperatures above and below T_g, with %strain of 0.70.

In Figures 3.1 (a) to 3.4 (a), we can see that G'(ω) always increases with frequency (ω) at various temperatures. The dependence on frequency of G'(ω) is lesser as the testing temperature is lower. This is expected because at a temperature above T_g, the terminal relaxtion consisting of a variety of length or time scale. At a temperature below T_g, α relaxation or the segmental motion predominantly exists and chain rigidity is hardly affected by the change in the time scale probed. We can also see that G'(ω) smaller for a higher temperature for a given frequency. At a temperature below T_g, any probing time or frequency scale used can only excite a local segment of the polymer chain where the total chain movement is prohibited and therefore rigidity is high. On the other hand, when the temperature is above T_g, a given time or frequency scale can influence a more variety of chain motion and therefore the rigidity is then reduced. Our observation here is consistent with the time-temperature superposition principle.

Figures 3.1 (b) to 3.4 (b) show plots of tan δ (G''/G') vs. frequency at various temperatures. At a temperature well above T_g, there is a tan δ peak which always occurs at a relatively low frequency. At a lower temperature, the tan δ is less well defined; there is a reduction in the tan δ magnitude as well as a horizontal shift in the peak towards a lower frequency. At a temperature below T_g, there are two tan δ peaks that can be observed: one at a low frequency and one at a high frequency. The low frequency peak can be identified with the single tan δ peak observed at a temperature above T_g, but its location is at a lower frequency. The high frequency peak shift instead to the left as temperature is lowered.

Tan δ (=G''/G') gives a ratio of the energy dissipated relative to the energy stored during the cyclic deformation of polymer when external force is applied. The low frequency is identified with the terminal relaxation or the transition from the entanglement plateau toward the flow or liquid-like regime.

On the other hand, the high frequency peak corresponds to the softening dispersion, α relaxation or the transition from the entanglement plateau towards the glassy regime. Therefore, we see and expect two peaks to occur for high molecular weight polymers. Only a single peak would exist for a low molecular weight polymer ($M_w < M_c$) because there is no entanglement plateau to be observed.

3.2 G'(ω) and tanδ(ω) Master Curves

The master curves of G'(ω) and tan δ for PMMA, SAN and their blend are shown in Figures 3.5- 3.8 respectively. The procedure for generating the master curves were given in details in chapter II. Here we will briefly mention the methodology. In our data, we have employed both the vertical and the horizontal shift factors. The vertical shift factor used is $b_T = T_o/T$ where T_o is the reference temperature (190 °C) and T is the testing temperature. We have not used the density correction [Ferry 1980]. The horizontal shift factor was then determined graphically from both G'(ω) and tan δ plots and the average value was taken as the final shift factor which was used to generate the master curves as well as determining the WLF contstants.

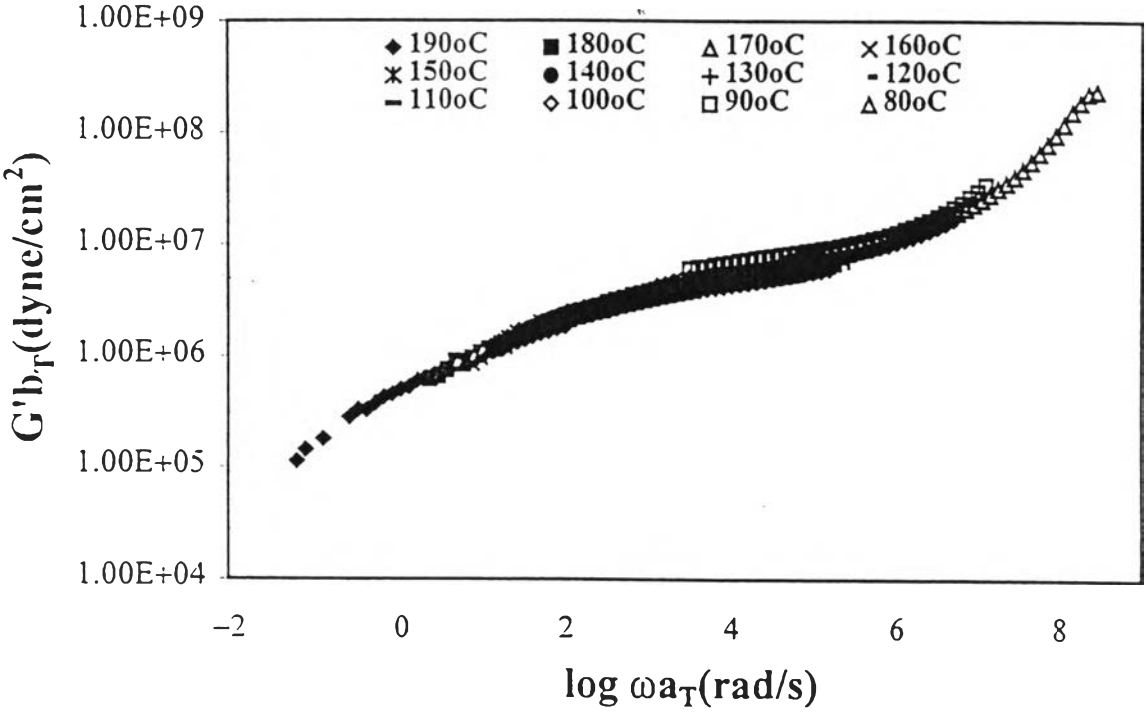

Figure 3.5 (a) G'(ω) master curve of PMMA M_w = 350000 $gmol^{-1}$. The reference temperature is 190°C.

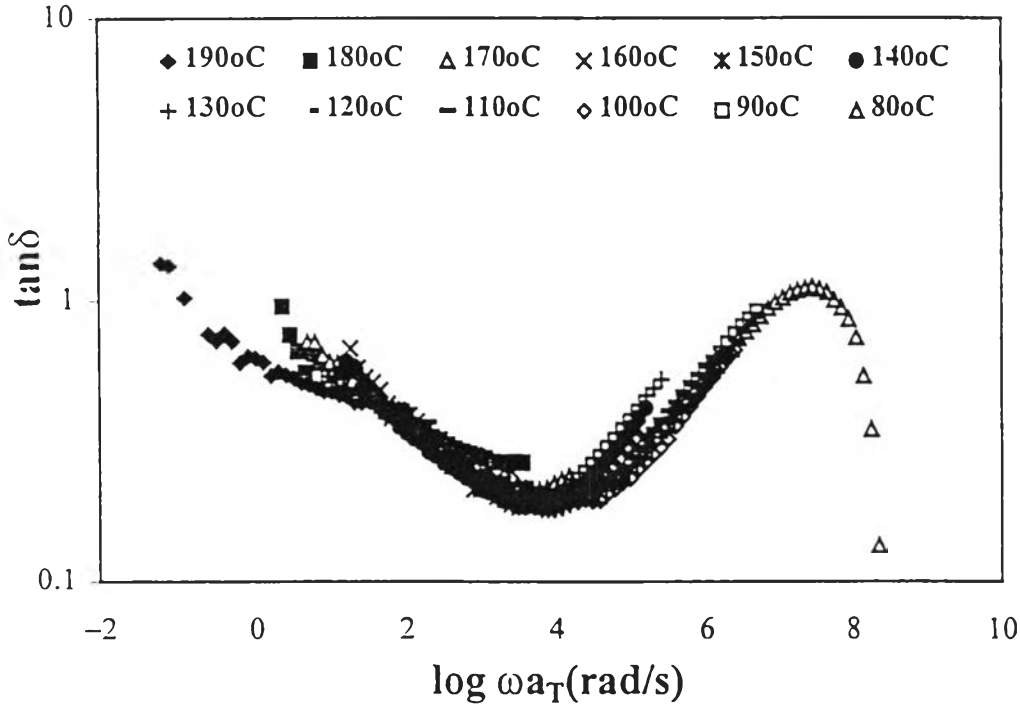

Figure 3.5 (b) tanδ(ω) master curve of PMMA M_w = 350000 $gmol^{-1}$. The reference temperature is 190°C.

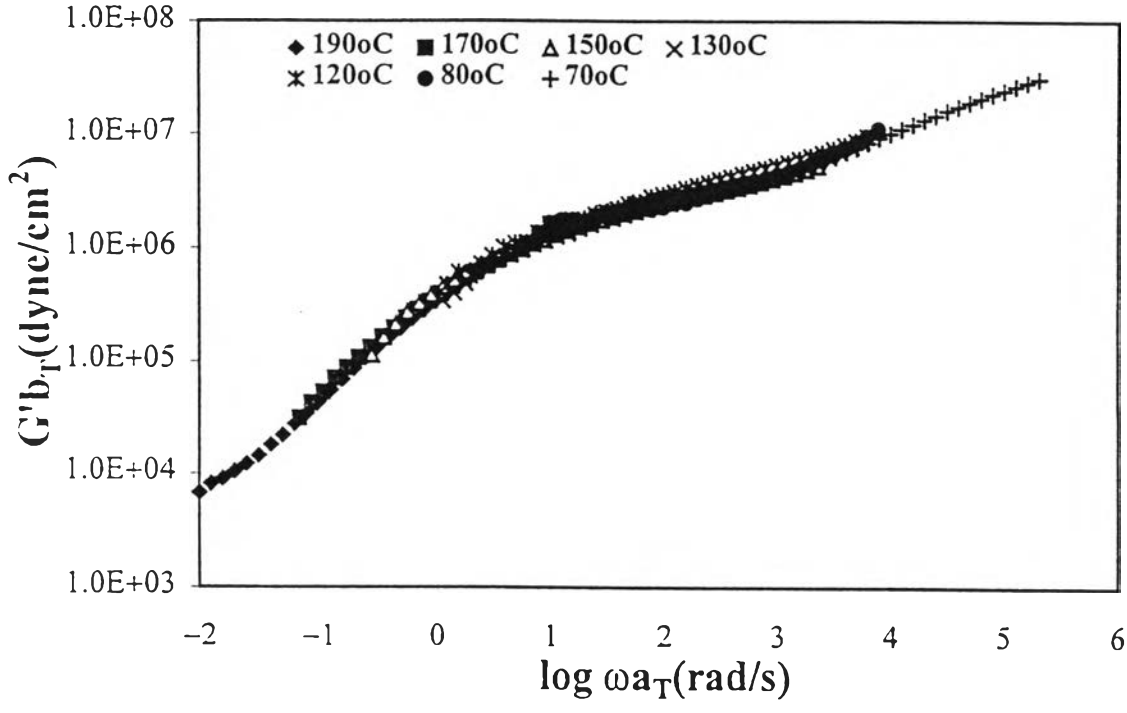

Figure 3.6 (a) G'(ω) master curve of PMMA M_W = 75000 $gmol^{-1}$. The reference temperature is 190°C.

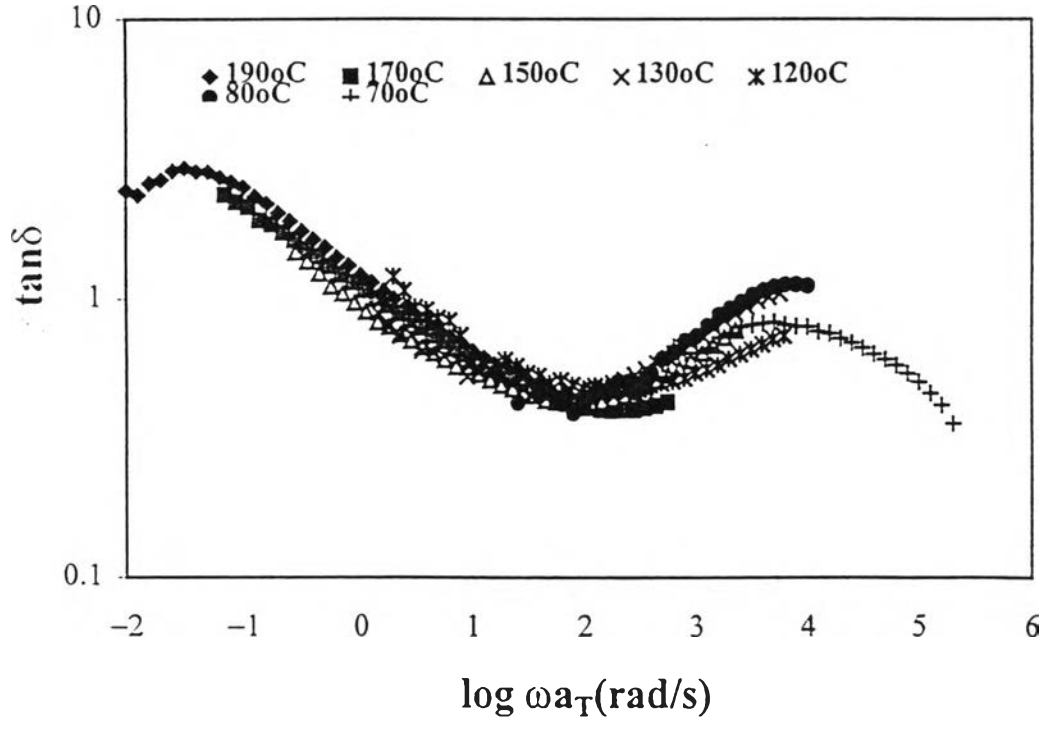

Figure 3.6 (b) tanδ(ω) master curve of PMMA M_W = 75000 $gmol^{-1}$. The reference temperature is 190°C.

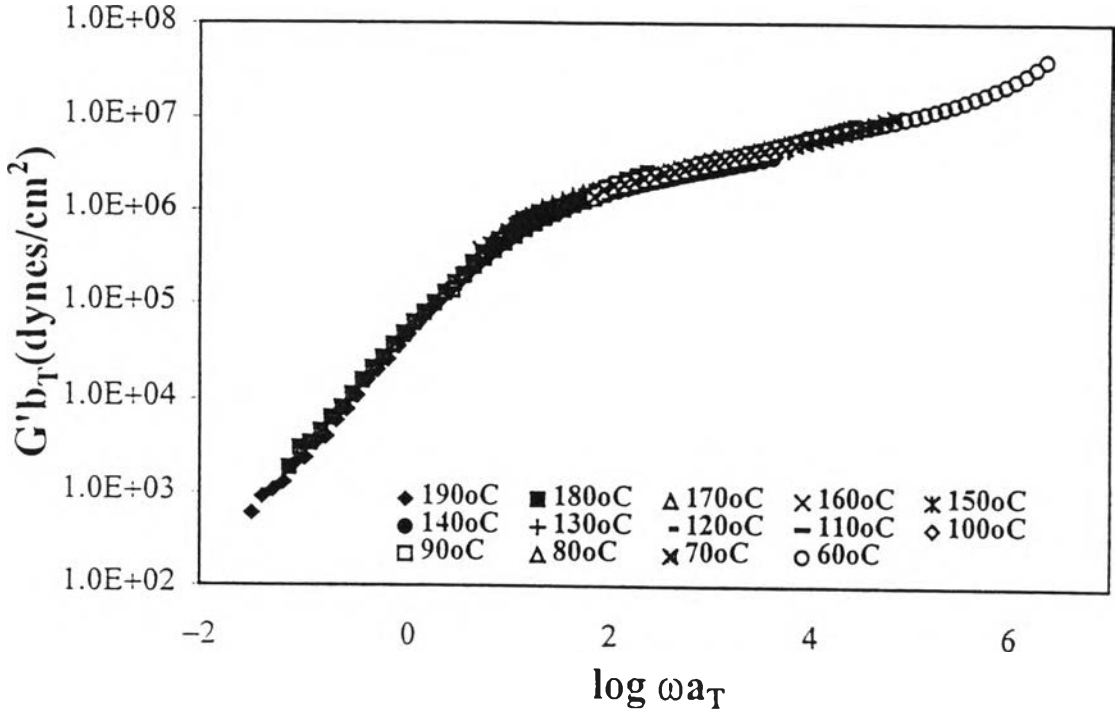

Figure 3.7 (a) G'(ω) master curve of SAN75:25. The reference temperature is 190°C.

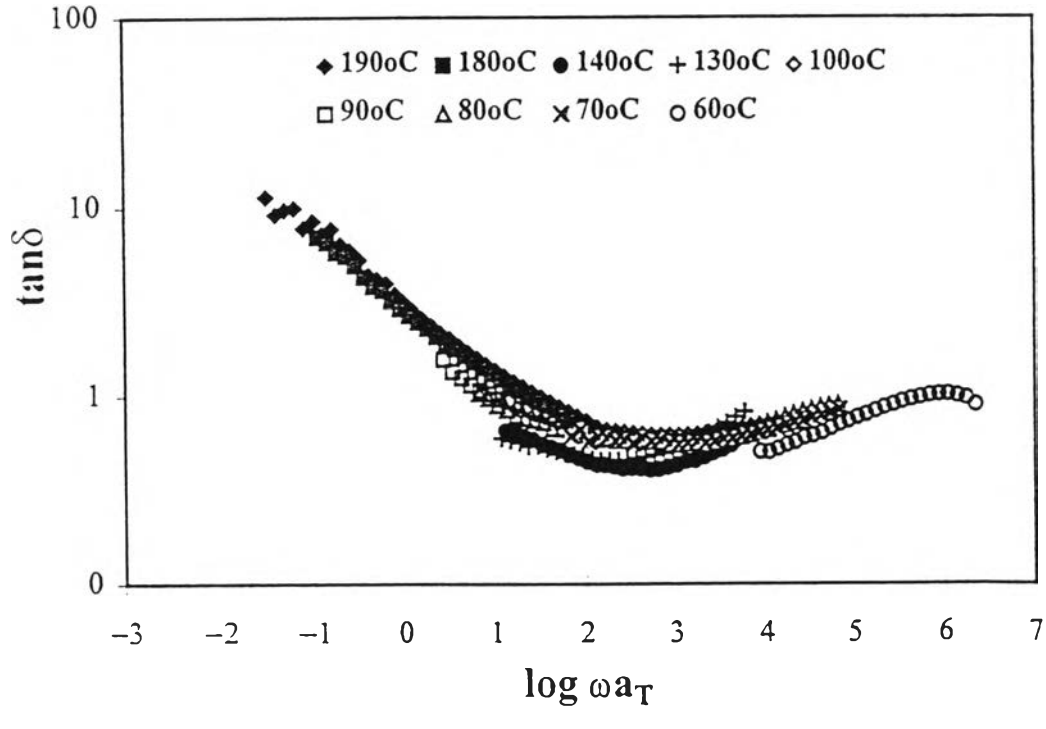

Figure 3.7 (b) tanδ(ω) master curve of SAN75:25. The reference temperature is 190°C.

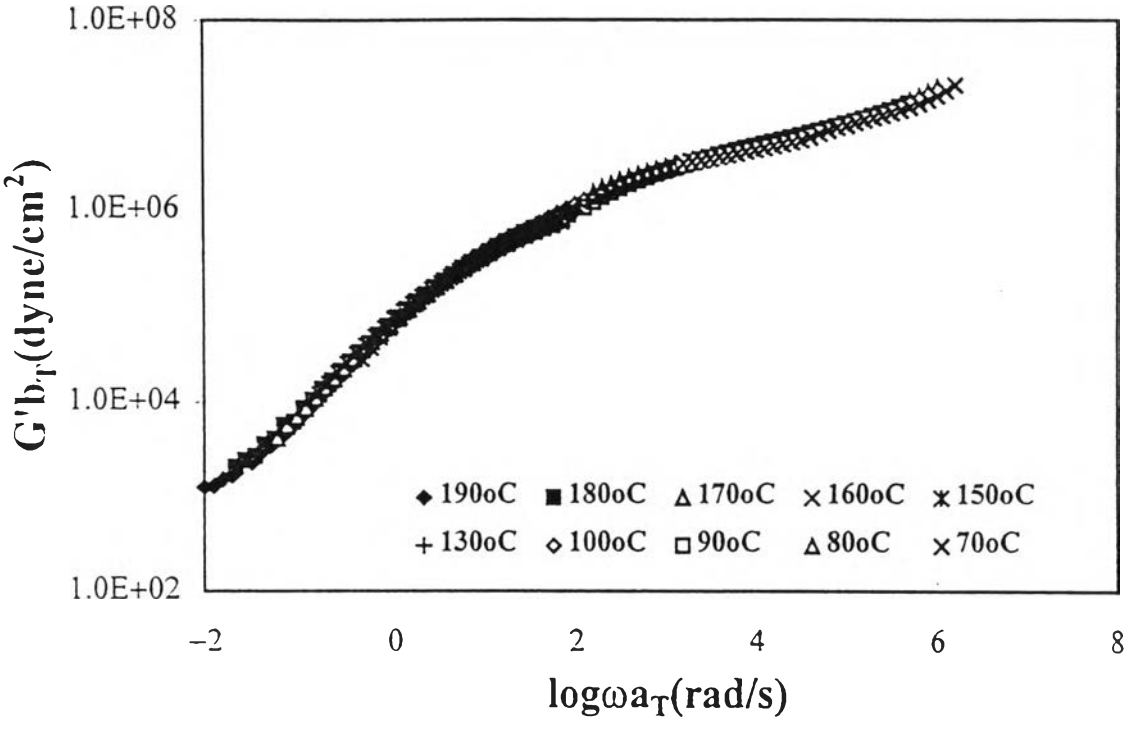

Figure 3.8 (a) G'(ω) master curve of PMMA/SAN 30/70 blends. The reference temperature is 190°C.

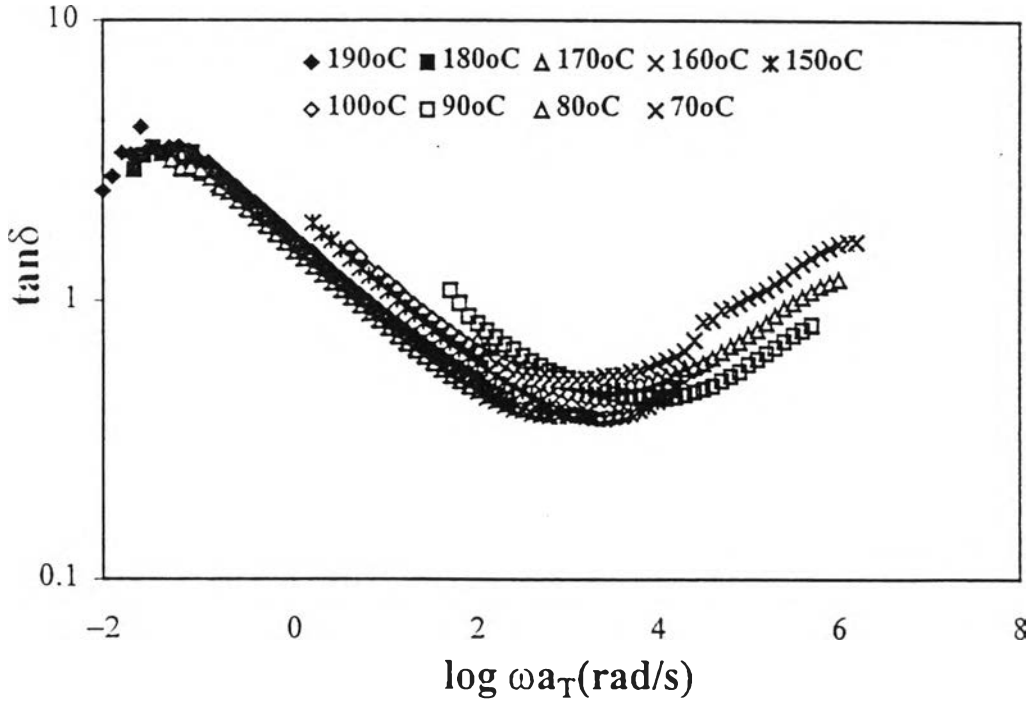

Figure 3.8 (b) tanδ(ω) master curve of PMMA/SAN 30/70 blends. The reference temperature is 190°C.

Figures 3.5 (a) - 3.8 (b) show the G'(ω) master curves of PMMA's, SAN and their blend respectively. We can see that three regimes can be easily observed: the terminal zone at low frequency, the entanglement zone at intermidiate frequency and the softening zone at the high frequency. We have not observed the glassy regime where a G'(ω) plateau occurs because of the instrument limitation on the maximum frequency and slippage between the polymer film and the parellel plate occurred as we lowered the temperature.
The terminal zone observed in the figure is of limited extent in frequency and we do not see the ω^2 dependence or the Rouse like behavior. This is because of an artifact of the procedure. For one sample, that we choose a constant strain amplitude which is in the linear viscoelastic regime for all temperatures causes the artifact to happen. The unsuitable strain amplitude for a fix temperature may provide incorrect value of G'(ω) because the elastic limit of a glassy polymer is much smaller than for a rubber

On the other hand, the softening dispersion zone or the transition from the entanglement plateau to the glassy zone can be easily observed in our data. Our data of all polymer samples show the $\omega^{1/2}$ dependence in the transition regime, consistent with the classical and universal scaling dependence [Ferry 1980].

Figures 3.5 (b) to 3.8 (b) show the tan δ master curves of PMMA's, SAN and their blend respectively. We can see that there are two well collapsed peaks, one at low frequency and one at high frequency, and a minimum between the two peaks. The low frequency peak occurs within the terminal zone where dissipative loss is relatively large with respect to the storage energy in the limit of lower frequency. The high frequency peak is identified with the the softening dispersion zone where polymer segmental motions are probed; their motions are relatively free in movement relative to the chain motion between entanglement loci in the entanglement zone, and the monomer

movements or conformation changes in the glassy zone. The minimum well corresponds to chain restrictions due to entanglement couplings. In this zone, the samples have a rubberlike behavior.

The success in preparing these master curves should be compared with the failure in preparing the master curve of high molecular weight atactic PP's [Plazek 1983], where they noted the noncollapse in the transition zone. However, for high molecular weight PIB's, they obtained the compliance master curves by reducing the data from the glassy zone to the terminal zone [Plazek et al. 1992]. Recently, G'(ω) and G"(ω) master curves for PS and for the unfractionated family of PS(1100)PMMNa(y) series were prepared successfully by Yoshikawa et al. in 1996. These master curves curves exibited the terminal, the rubbery plateau, and the transition zones.

3.3 Effect of Molecular Weight on the Master Curves

Figure 3.9 shows PMMA G'(ω) master curves of two different molecular weights. The reference temperature is the same, namely 190 °C. In the terminal zone, we can see that the master curves do not collapse; G'(ω) of a higher molecular weight PMMA is larger than that of the lower molecular weight PMMA. This is an expected result that a larger molecular weight polymer has a wider frequency range encompassing the entanglement plateau. In the limit of a large mismatch in molecular weight, we expect the difference in the terminal to be more pronounced. Another physical explanation can also be provided; a shorter chain can reptate faster and the entanglement density is of a lesser degree.

In the rubberry zone or the entanglement plateau region, the master curves do collapse partially. The difference in G'(ω) in this zone may cause

from preparation technique. The polymeric specimen was prepared from solution, so the polymer morphology can be affected by the solvent. As can be seen from the figure, the width of the plateau depends strongly on molecular weight. The higher molecular weight PMMA (M_w = 350000 $gmol^{-1}$) has more entanglement networks to restrict the chain motions than those of the lower one (M_w = 75000 $gmol^{-1}$). The rubbery plateau region of the higher molecular weight polymer is wider than the lower one. Therefore, for entangled linear polymers, the higher the molecular weight of the polymer, the wider its rubbery plateau region is. This rubbery plateau region is found to appear only when the molecular weight exceeds the critical molecular weight (M_c) which is about twice the entanglement molecular weight (M_e). PMMA has M_c and M_e of 27500 and 10000 respectively [Bailey et al. 1981]. Since our PMMA's samples have molecular weights greater than M_c, both PMMA's show the rubbery plateau region.

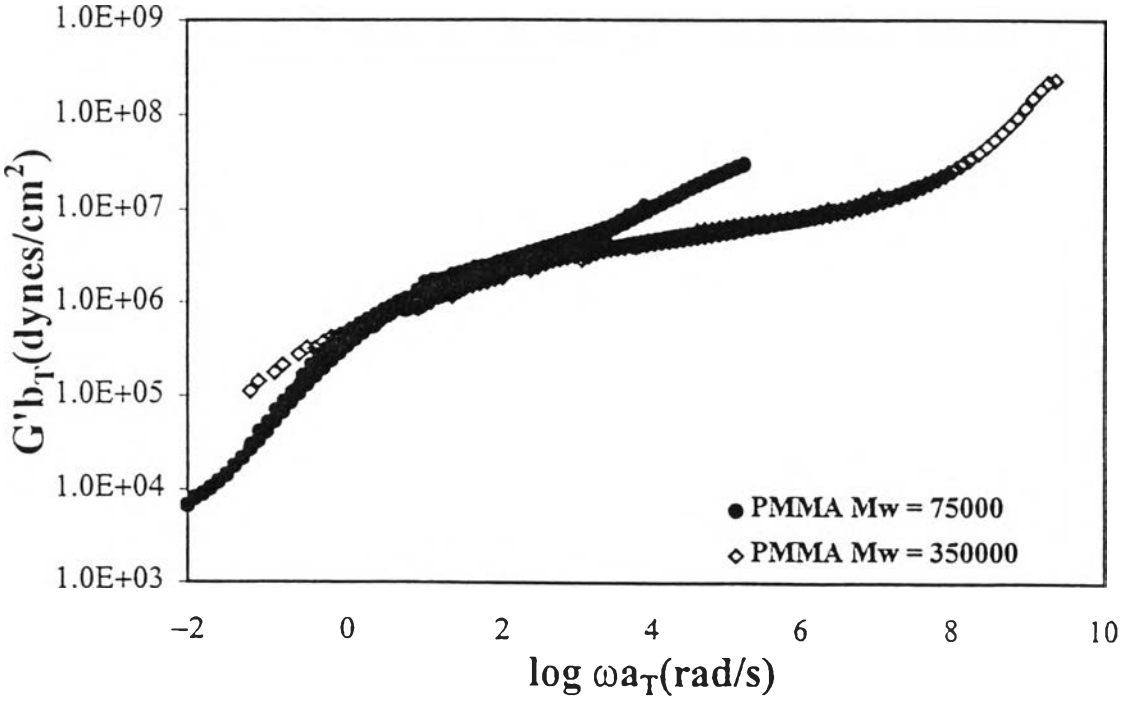

Figure 3.9 G'(ω) master curves of two different molecular weights of PMMA's.

We note that the plateau moduli (G_N^o) of the two PMMA's of different molecular weights are nearly the same, having a value of about $1.4x10^6$ dynes/cm^2. The plateau modulus G_N^o is therefore molecular weight independent. The molecular weight independence of G_N^o for the narrow molecular weight distriburtion polystyrenes was reported by Plazek and Agarwal (1978). For the narrow molecular weight distribution polybutadienes, it was reported by Palade et al. (1995). Their results and our are consistent with the Doi and Edwards's theory which proposed that G_N^o is independent of M_w but inversely proportional to M_e .

The transition zone is normally associated with a large change in the modulus as frequency is changed. In the transition zone, we can only expect the segmental motion which, in principle, should be independent of the molecular weight. We do find that $G'(\omega)$ of all our samples have the same $\omega^{1/2}$ dependence. However, the onset of the transition zone occurs at a frequency which appears to depend on molecular weight.

Our result should be contrasted with the $G'(\omega)$ and $G''(\omega)$ master curves of polybutadiene samples with different molecular weights [Palade et al.1995]. They noted that in the glassy and the transition zones, the master curves collapsed to be a single master curve. Moreover, Graessley and Roover (1979) showed that the $G'(\omega)$ master curves of star-branched polystyrenes with different molecular weights collapsed to form a single master curve in the transition zone.

The inability to find a collapse of the master curves in the transition zone can be explained as follows; the two different molecular weight polymer may have different M_e because of the poor sample preparation and M_e is solvent dependent. Therefore, both M_e and M_c are molecular weight dependent. Alternatively, the disagreement between our result and those in the literature can be described in the framework of molecular weight distribution of the

polymer. Although the α-relaxation in the transition zone does not depend on the molecular weight of polymer , it depends strongly on the polymer structure [Alegria et al. 1991]. For two polymers of the same type with either the same or different molecular weight, the molecular weight distributions of the samples can cause the coupling between local chains of different length and therefore a cooperative effect and/or a complexity of the system to be quite different. If the polymer investigated was polydisperse, the complexity of the system would be higher than the monodisperse one because of the different distributions in relaxation time. The coupling parameter β_α giving a measure of the coupling between the segmental motions should be higher for a wider molecular weight distribution. The shift factor $(a_T)_\alpha$ related to the shifting of relaxation time scale should be higher also. Therefore, the master curves of the same polymer with different molecular weight distributions may not collapse to form a single master curve in the glassy and the transition zones.

3.4 Master Curve of the PMMA/SAN Blend

The G'(ω) master curves of PMMA (M_w= 75,000), SAN and their blend are shown in Figure 3.10. The reference temperature is 190 °C. We can see that the blend master curve has three zones: the terminal zone, the entanglement zone and the transition zone, similar to the master curves of the pure components. The blend master curve is very close to the master curve of SAN; this is because the blend composition was PMMA /SAN : 30/70. The blend master curve is bound from above by the PMMA master curve and from below by the SAN master curve; an exception occurs in the entanglement zone where the blend master curve falls below that of SAN. The reason for this is unclear but it's possible that the exothermic interaction between PMMA and SAN is

different from that of PS and acrylonitrile inducing a larger M_e and a lower G_N^o.

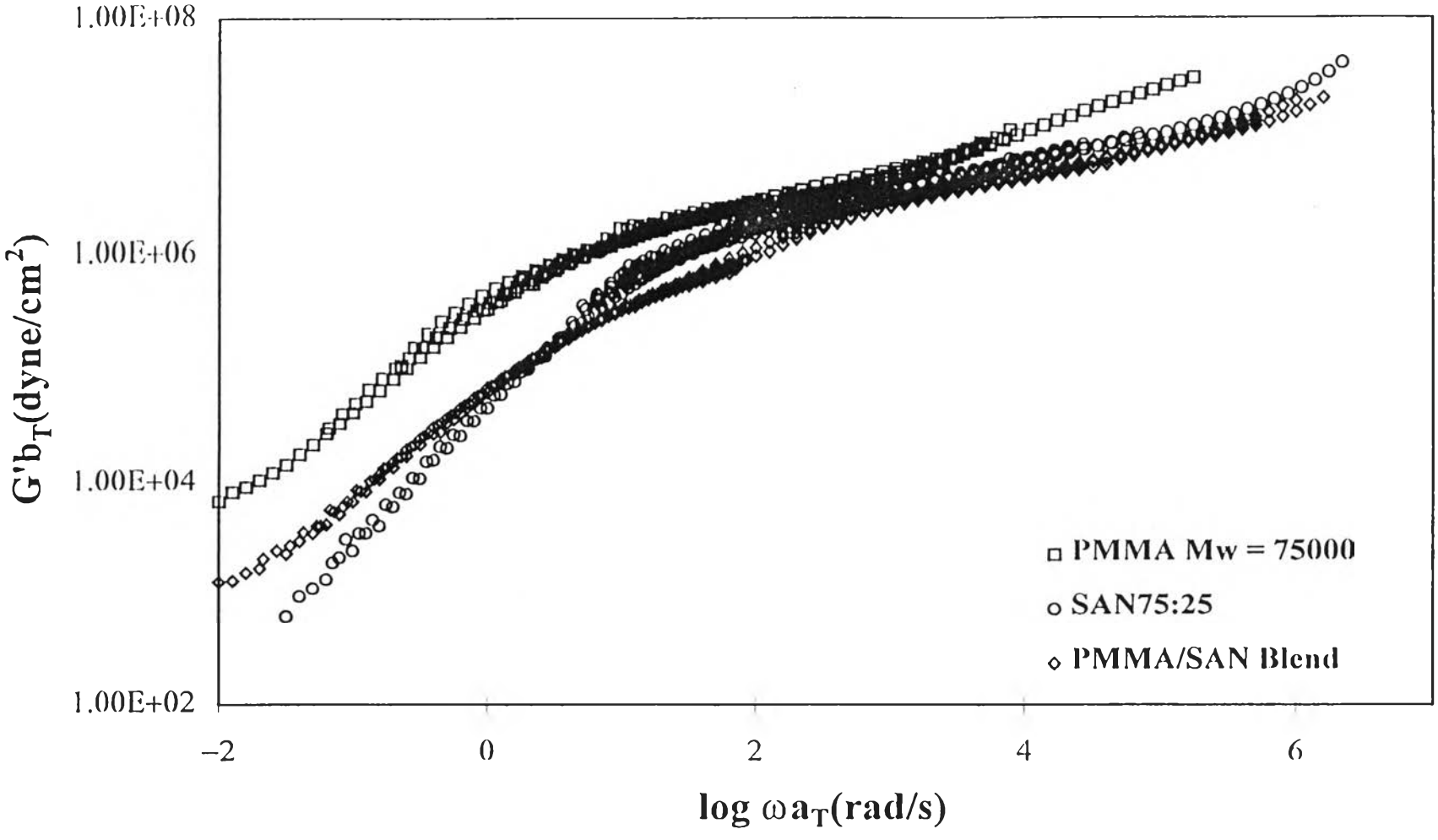

Figure 3.10 G'(ω) master curve of PMMA M_W = 75000 gmol^{-1}, SAN75:25 and PMMA/SAN 30/70 blend. The reference temperatuere is 190 °C.

3.5 Shift Factors above and below T_g

The empirical horizontal shift factors used for preparing the $G'(\omega)$ master curves of PMMA, SAN, and their blend are shown in Figures 3.11, 3.12, and 3.13 respectively. The reference temperature is 190 °C. T_g's for our samples are 92-99 °C, 88 °C for PMMA and SAN respectively. The miscible blend T_g is 86° C. We can see from these figures that there are two regimes for log a_T vs. T : one above T_g and one below T_g.

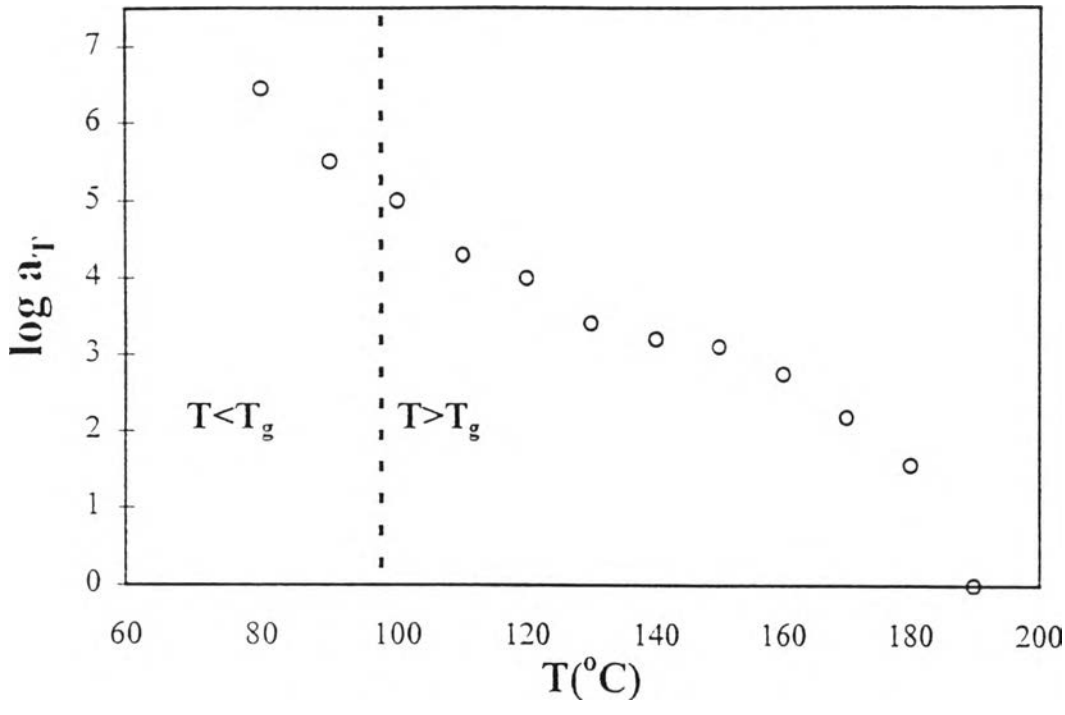

Figure 3.11 (a) Empirical shift factors vs. temperatures above and below T_g of PMMA M_W = 350000 $gmol^{-1}$. The reference temperarure is 190 °C.

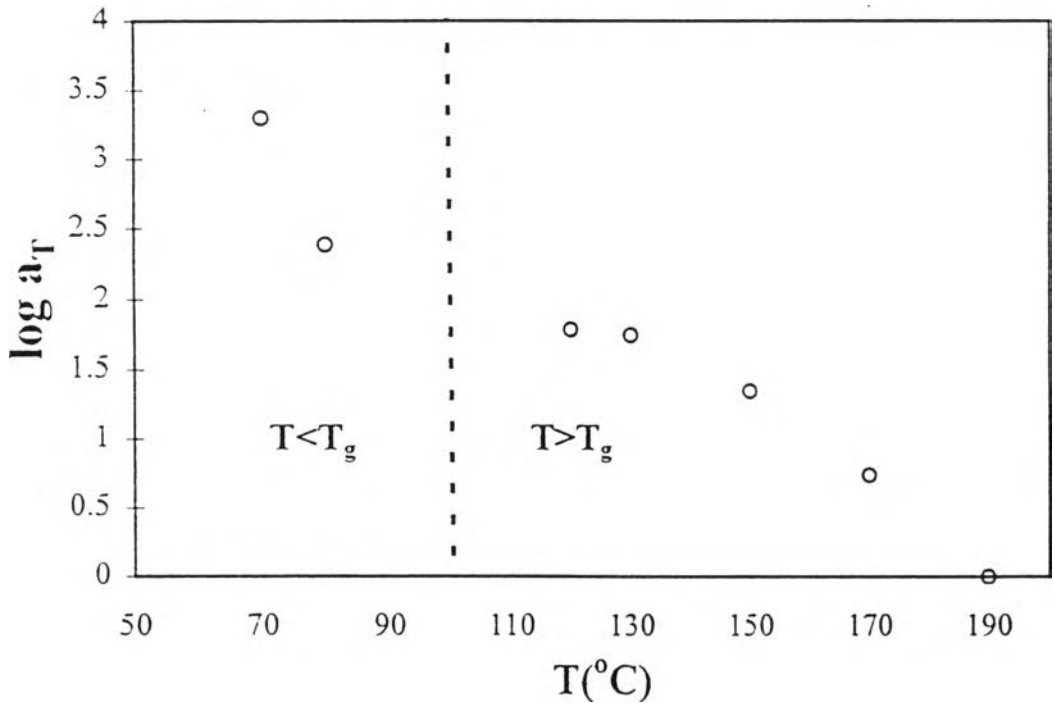

Figure 3.11 (b) Empirical shift factors vs. temperatures above and below T_g of PMMA M_W = 75000 $gmol^{-1}$. The reference temperature is 190 °C.

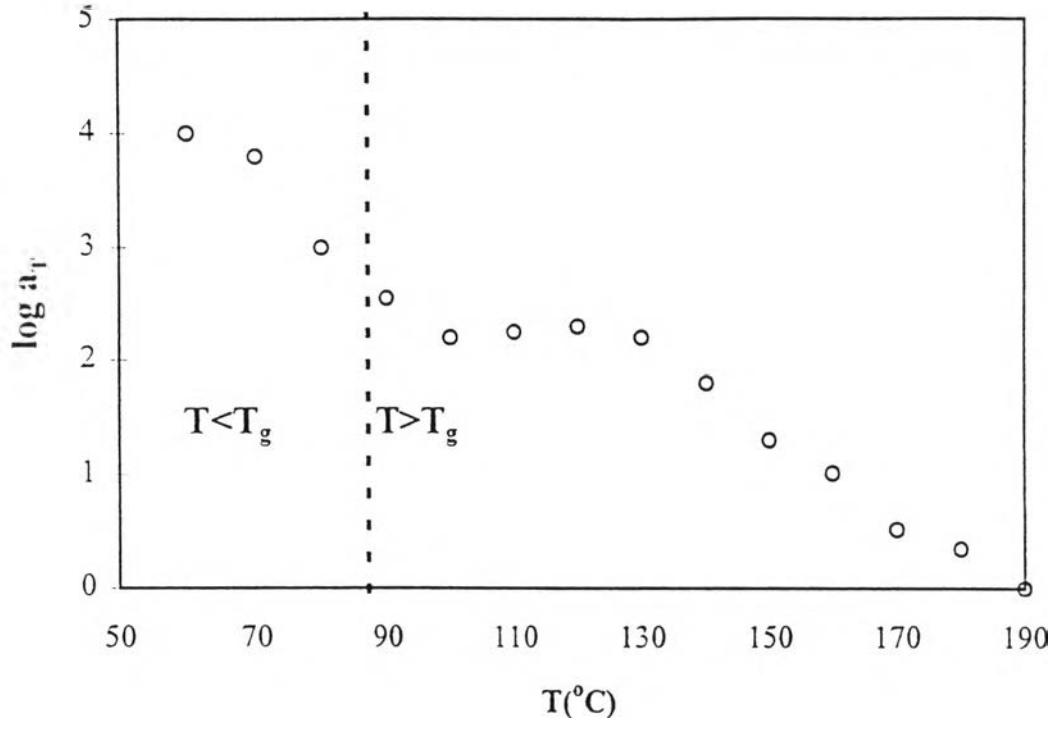

Figure 3.12 Empirical shift factors vs. temperatures above and below T_g of SAN75:25. The reference temperature is 190 °C.

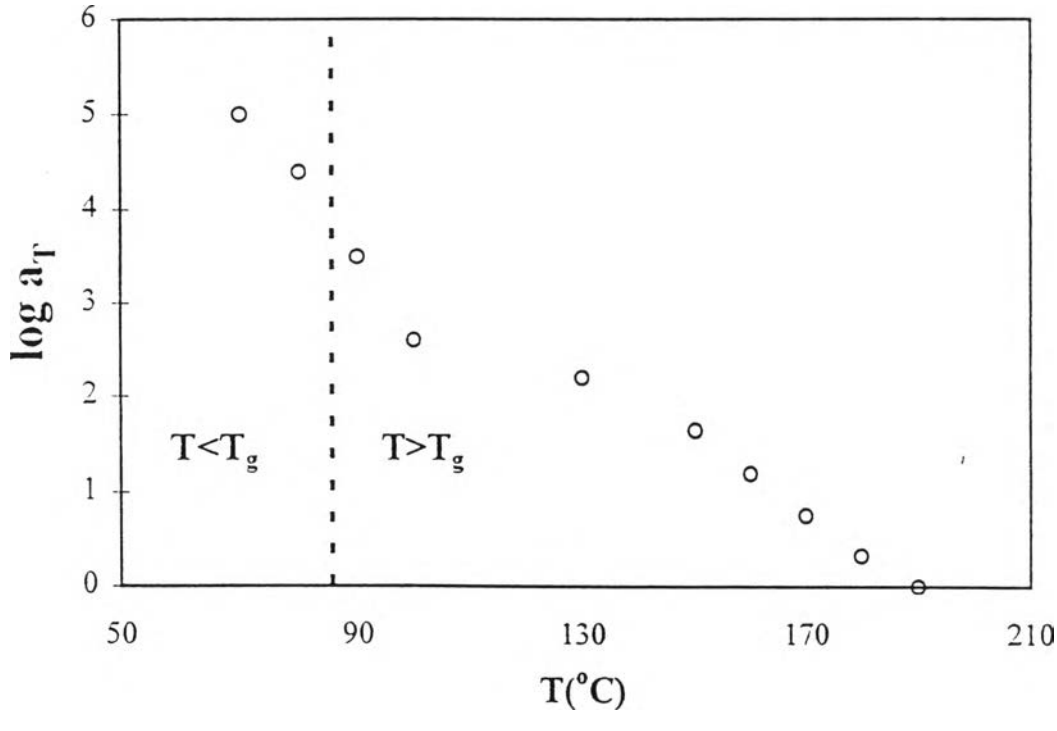

Figure 3.13 Empirical shift factors vs. temperatures above and below T_g of PMMA/SAN 30/70 blend. The reference temperature is 190 °C.

In Figures 3.11 - 3.13, we can see that the plots of log a_T vs. T below T_g show a stronger temperature dependence than the plots of log a_T vs. T above T_g. This result is consistent with the well known fact that below the glass transition temperature the free volume is relatively small and therefore a small change in the thermal energy can drastically change the time scale ratio. On the other hand, above the glass transition temperature, the free volume is large and a polymer chain is in equilibrium and free to move. A change in the thermal energy must be relatively considerable to make a noticeable change in the time scale ratio. It was shown experimentally by Cavaille et al. in 1987 that different relaxations and/or absorption processes of a polymer respond with different sensitivities to temperature. Their result is in good agreement with our results. In fact, different temperature dependences of the shift factor of the α-relaxation and the terminal relaxation have been reported by several authors in the past along time [Plazek 1982, Ngai & Plazek 1986, Cavaille et al. 1987, Alegria et al. 1991, Ngai et al. 1992, Palade et al. 1995]. We may summarize this section by saying that the shift factor can be categorized as $(a_T)_\alpha$ and $(a_T)_\eta$ for the α relaxation below T_g and the terminal relaxation above T_g.

3.6 Shift Factors and the WLF Equation

The temperature dependence of $(a_T)_\eta$ above T_g (terminal zone) is usually analyzed in the framework of the free volume theory [Ferry 1980]. The William-Landel-Ferry (WLF) equation is the empirical equation used to express the temperature dependence of $(a_T)_\eta$ above T_g. The WLF equation derived in the framework of free volume theory is :

$$\log a_T = \log(\lambda/\lambda_o) = -C_1^o(T-T_o)/C_2^o + T-T_o, \qquad (3.1)$$

where C_1^o and C_2^o are constants at the reference temperature T_o. The shift factor data of Figures 3.11- 3.13 were fitted according to equation (3.1) above and the constants C_1^o and C_2^o were determined and shown in Table 3.1. We note that the constants are negative contrary to typical positive values often found in literature. This is simply because we have used the reference tempaerature well above T_g. The shift factors were then calculated by the WLF equation and plotted versus temperatures for all our samples, as shown in Figures 3.14, 3.15, and 3.16. We can see that the WLF equation can fit the data quite well as long as temperature is above T_g. At temperature below T_g, the temperatue dependence of (a_T) does not follow the free volume theory or the emperical WLF equation.

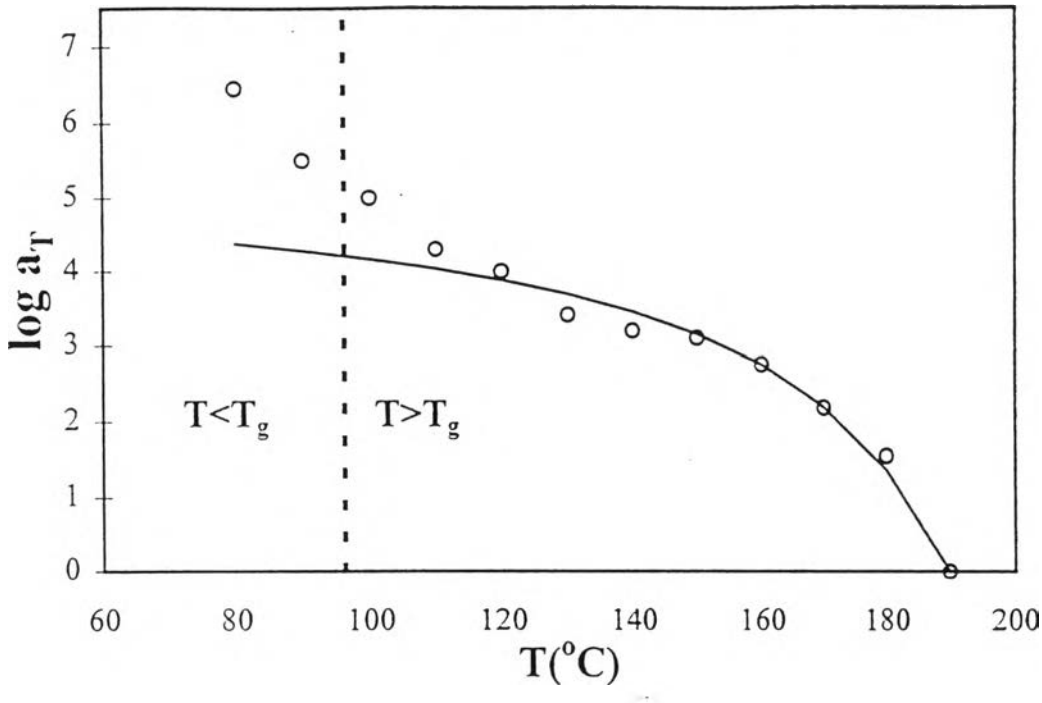

Figure 3.14 (a) The open circles are apparent shift factors a_T of PMMA M_W = 350000 $gmol^{-1}$. The solid line is the WLF equation. The reference temperature

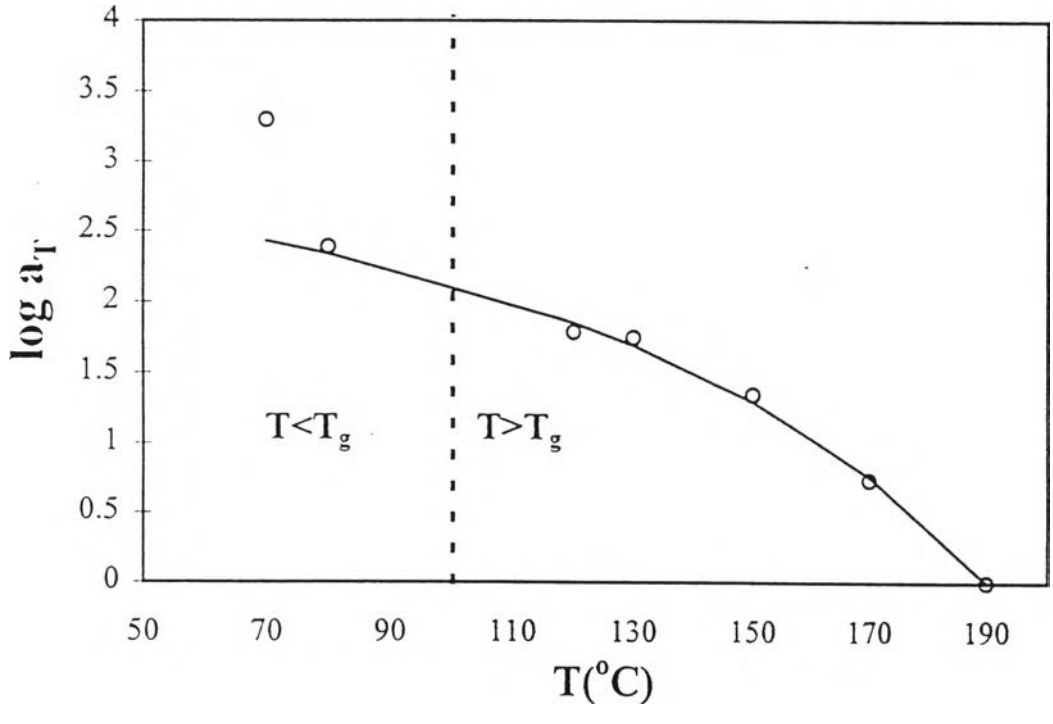

Figure 3.14 (b) The open circles are apparent shift factors a_T of PMMA M_W = 75000 $gmol^{-1}$. The solid line is the WLF equation. The reference temperature is 190 °C.

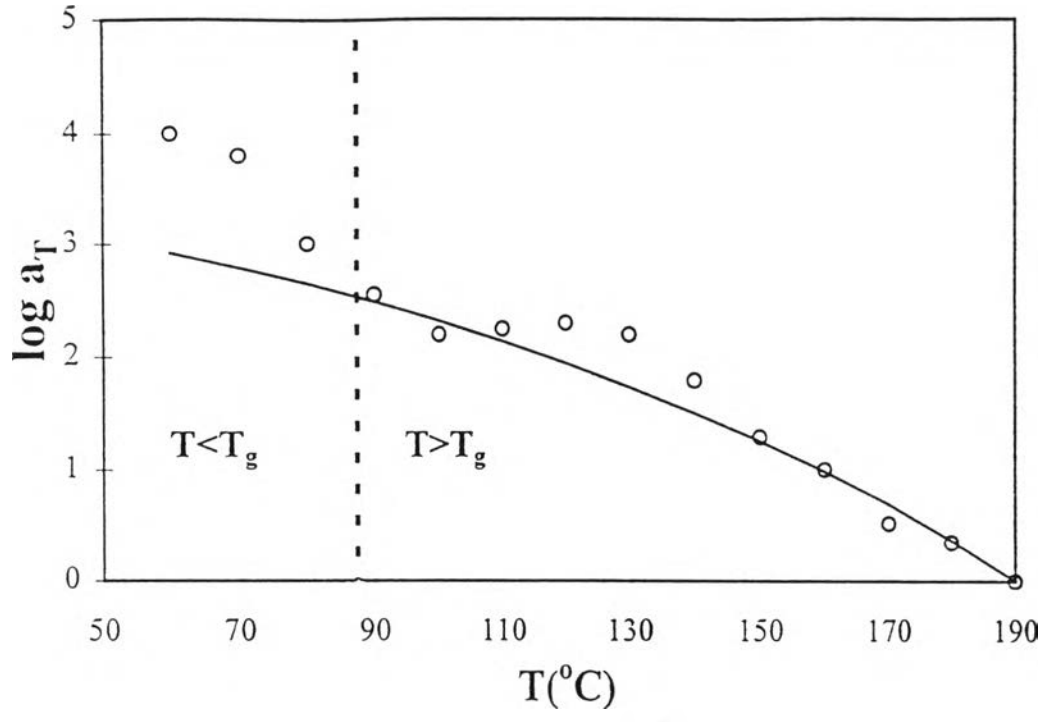

Figure 3.15 The open circles are apparent shift factors a_T of SAN75:25. The solid line is the WLF equation. The reference temperature is 190 °C.

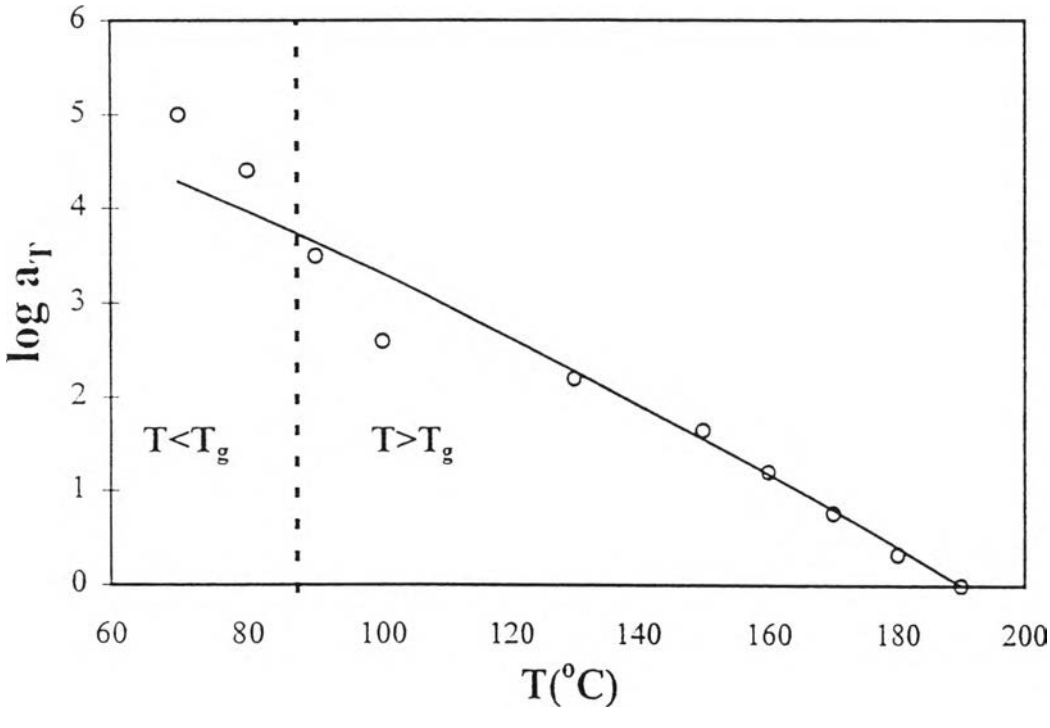

Figure 3.16 The opened circles are apparent shift factors a_T of PMMA/SAN 30/70 blend. The solid line is the WLF equation. The reference temperature is 190 °C.

Table 3.1 The constants C_1^o and C_2^o of different polymer systems. The reference temperature is 190 °C

Polymer System	C_1^o	C_2^o
PMMA M_w = 350000 $gmol^{-1}$	-5.6	-31.4
PMMA M_w = 75000 $gmol^{-1}$	-4.3	-92.3
SAN 75:25	-6.9	-181.3
PMMA/SAN 30/70 Blend	-34.8	-856.9

3.7 The Coupling Model of Relaxation

We have found that $(a_T)_\alpha$ shows a different temperature dependence from that of $(a_T)_\eta$, and the WLF equation could only be used to fit empirical $(a_T)_\eta$ data. Therefore the α relaxation involves different molecular motion or physics than those of the terminal relaxation. Previous investigators [Plazek, 1982] have shown that the α relaxation temperature dependence can be succesfully fitted to the VFTH equation. Instead, we will attempt to examine and apply the Coupling model to our $(a_T)_\alpha$ data based on the $(a_T)_\eta$ data and the fitted WLF equation.

The coupling model of relaxation dictates the relation between the two corresponding shift factors above and below T_g [Ngai & Plazek, 1986] is given by:

$$\beta_\eta \log(a_T)_\eta = \beta_\alpha \log(a_T)_\alpha . \qquad (3.2)$$

Since the molecular processes are different at above and below T_g, the related coupling parameters β_η and β_α are expected to be different.

3.7.1 Stress Relaxation Measurements

Stress relaxation quantity in a complex system is given by [Williams. 1991]:

$$G_R(t) = G_R(o)\exp[-(t/\tau^*)^{\beta}] , \qquad (3.3)$$

β is the stretched exponent and τ^* is the relaxation time time scale at a given temperature. They can be determined from a best fit of the fractional exponential of Kohraush (equation 3.3) to the stress relaxation measurements. We plotted $\ln G_R(t)$ vs. t^{β} at various β's in range given by Ngai and Plazek (1986). The plot which yeilded the best straight line and fitting coefficient at each temperature was chosen with the corresponding β. The slope of the straight line gives us $-(1/\tau^*)^{\beta}$. τ^* was obtained from the slope with the known β.

The stress relaxation measurements of the two PMMA's, SAN 75:25, and PMMA/SAN 30/70 blend were carried at various temperatures spanning above and below T_g. Some examples of the stress relaxation measurements are shown in Figures 3.17- 3.23.

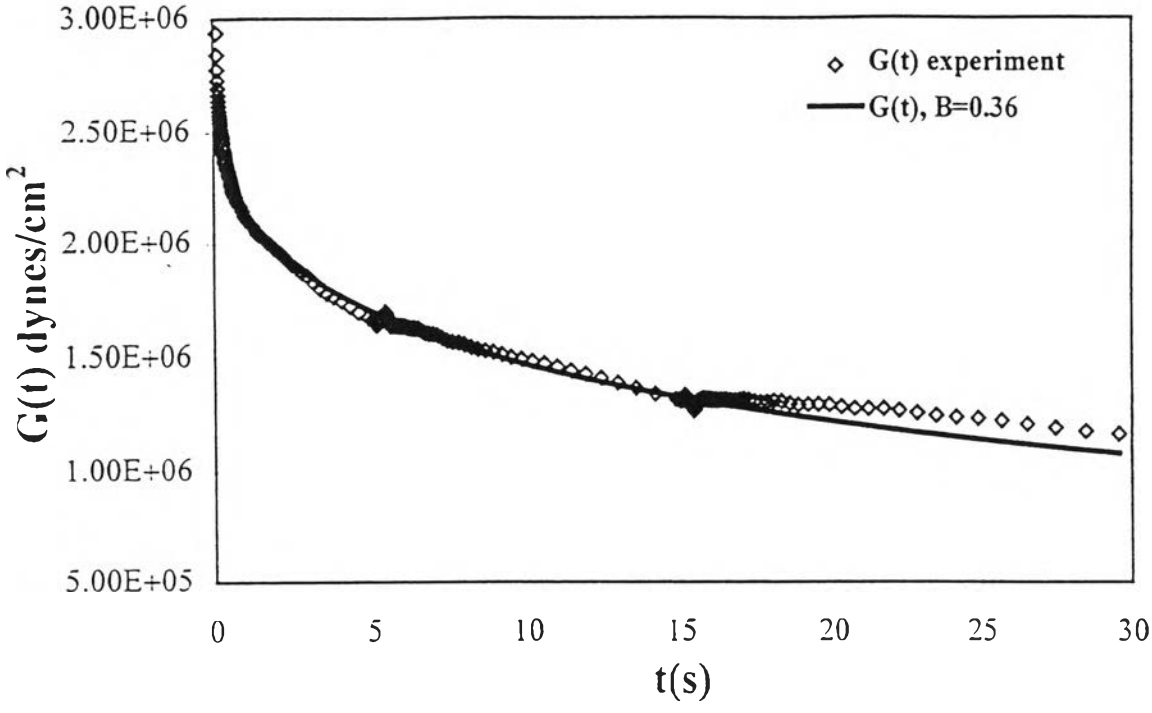

Figure 3.17 (a) Open diamonds are relaxation moduli vs. time of PMMA M_W = 350000 $gmol^{-1}$ at 130 ^oC with % strain of 0.3. Solid line is the theoretical stress relaxation moduli with $\beta = 0.36$.

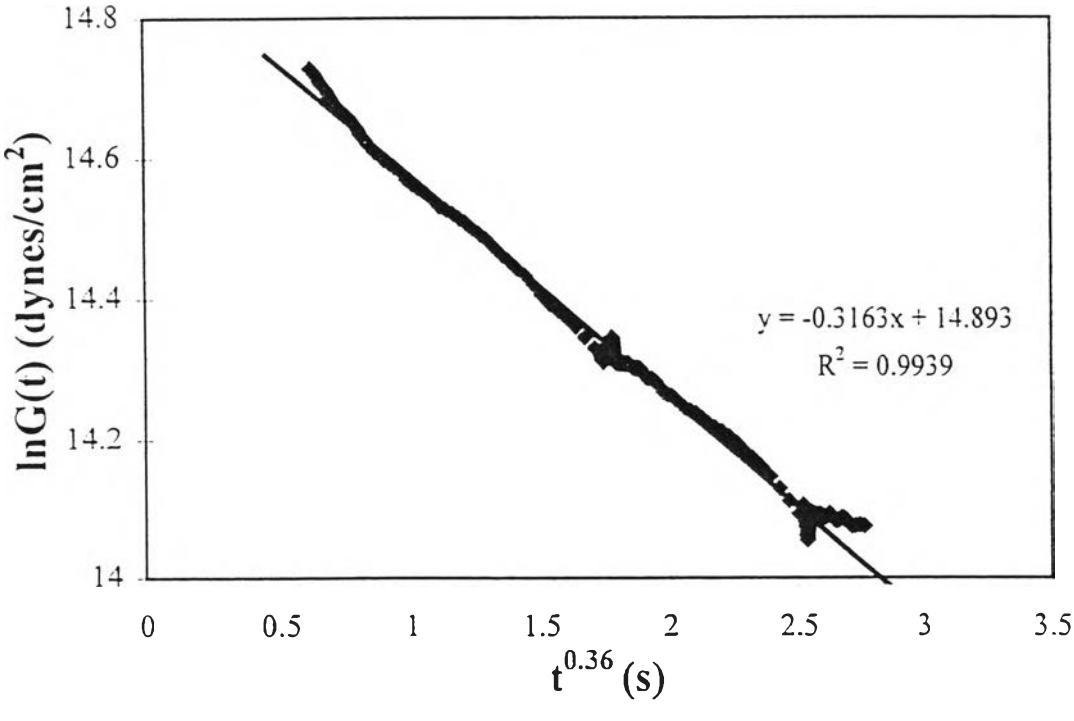

Figure 3.17 (b) The plot of $\ln G_R(t)$ vs. t^{β} of PMMA M_W = 350000 $gmol^{-1}$ at 130 ^oC with β of 0.36.

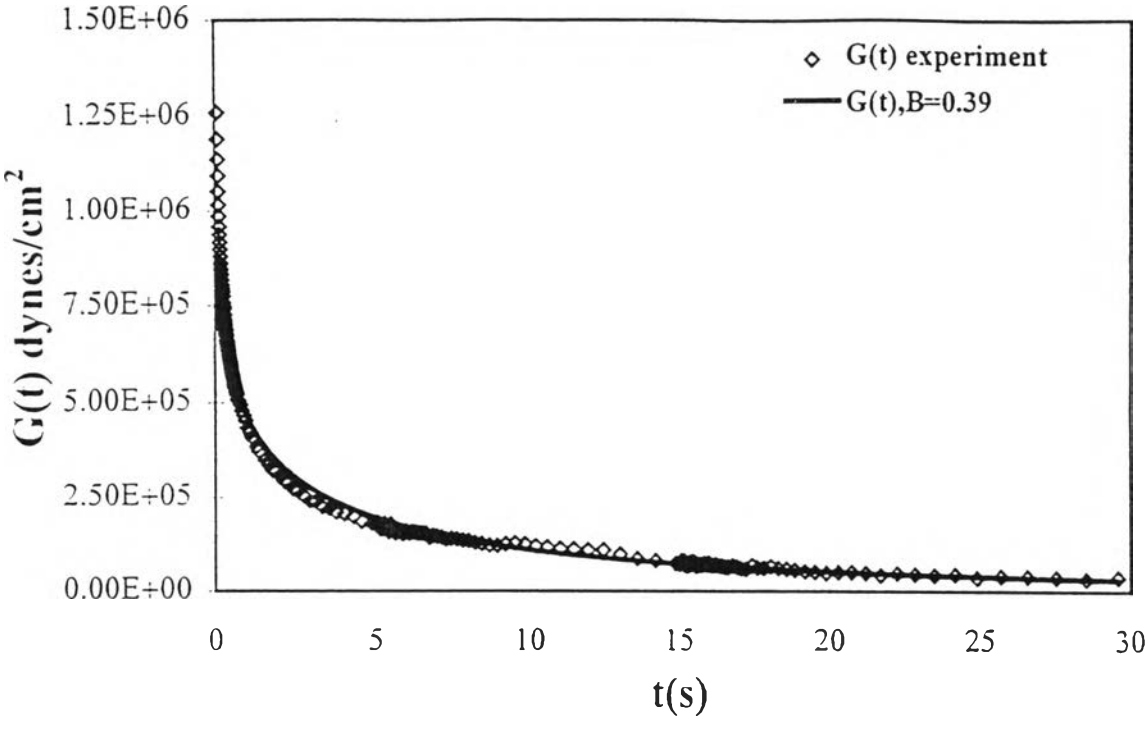

Figure 3.18 (a) Open diamonds are relaxation moduli vs. time of PMMA M_w = 75000 gmol^{-1} at 130 °C with %strain of 0.3. Solid line is the theoritical stress relaxation moduli with $\beta = 0.39$.

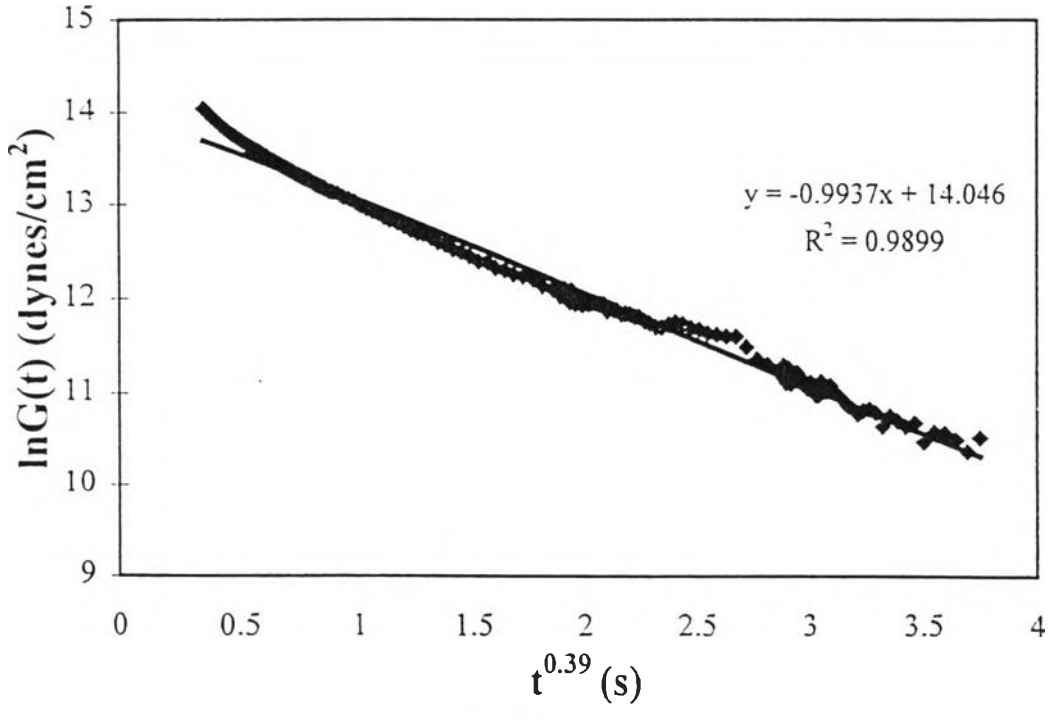

Figure 3.18 (b) The plot of $\ln G_R(t)$ vs. t^{β} of PMMA M_w = 75000 gmol^{-1} at 130 °C with β of 0.39.

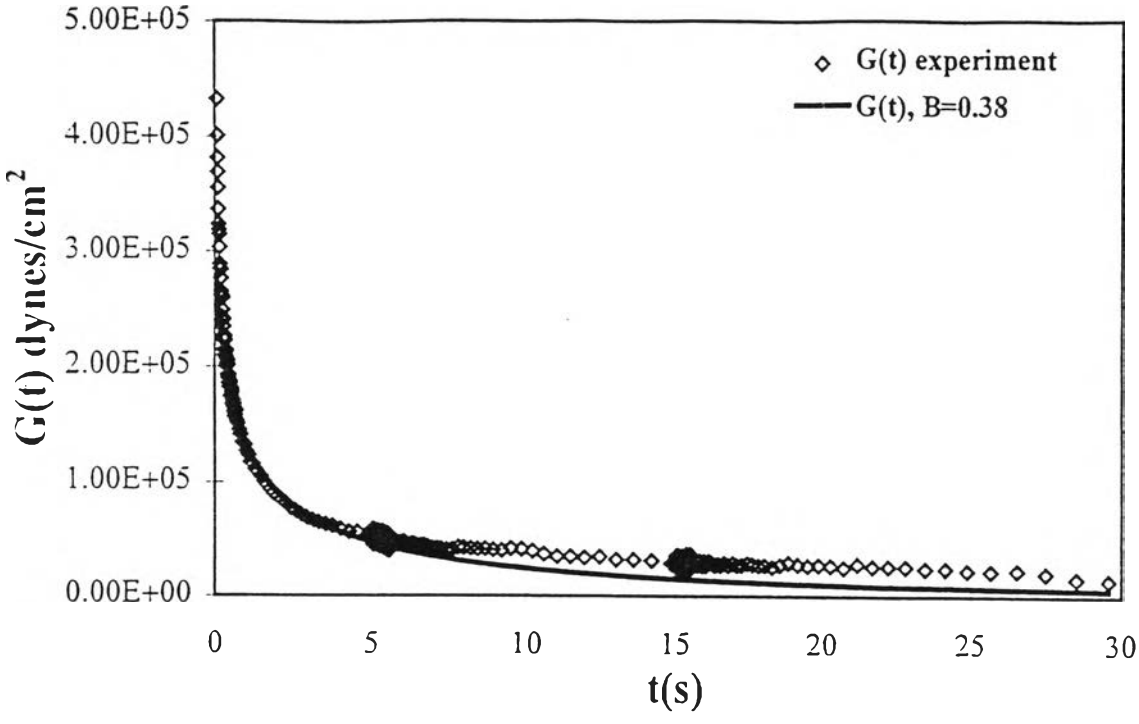

Figure 3.19 (a) Open diamonds are relaxation moduli vs. time of SAN 75:25 at 130 °C with %strain of 0.3. Solid line is the theoritical stress relaxation moduli with $\beta = 0.38$.

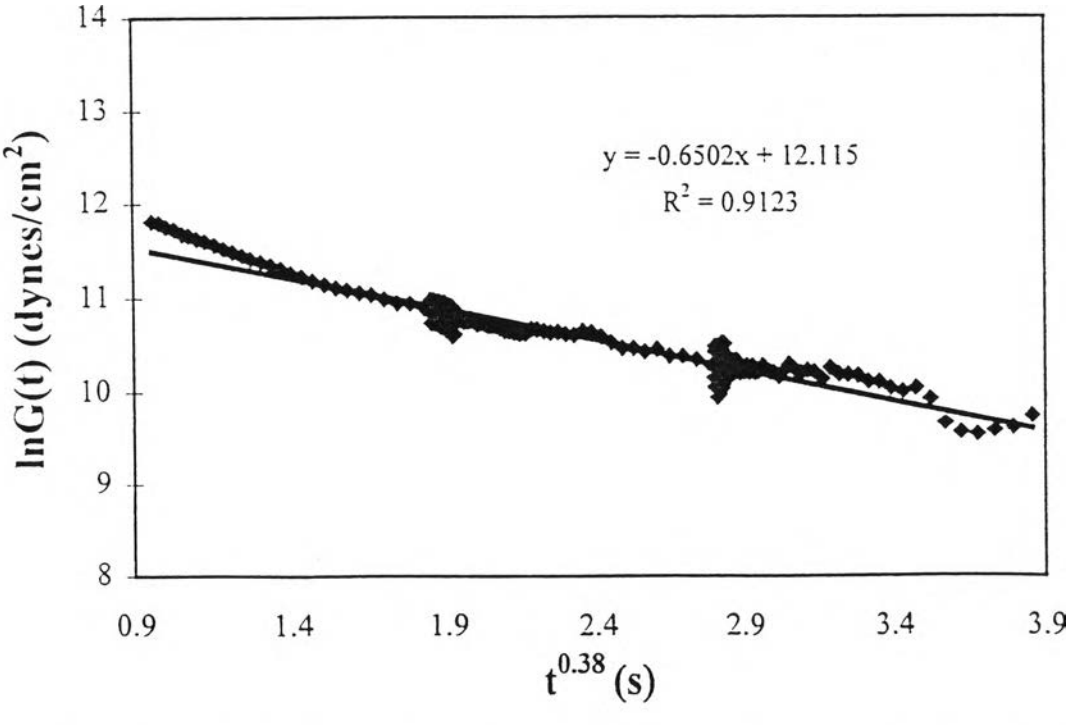

Figure 3.19 (b) The plot of $\ln G_R(t)$ vs. t^{β} ofSAN 75:25 at 130 °C with β of 0.38.

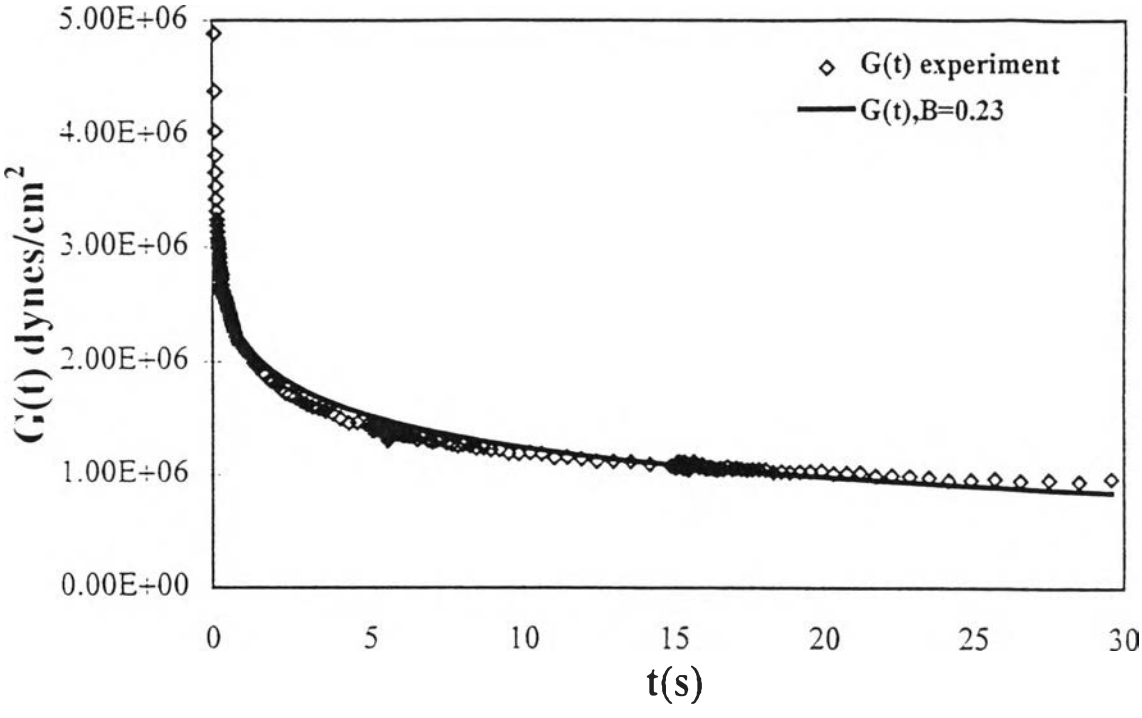

Figure 3.20 (a) Open diamonds are relaxation moduli vs. time of PMMA/SAN 30/70 blend at 130 °C with %strain of 0.3. Solid line is the theoritical stress relaxation moduli with $\beta = 0.23$.

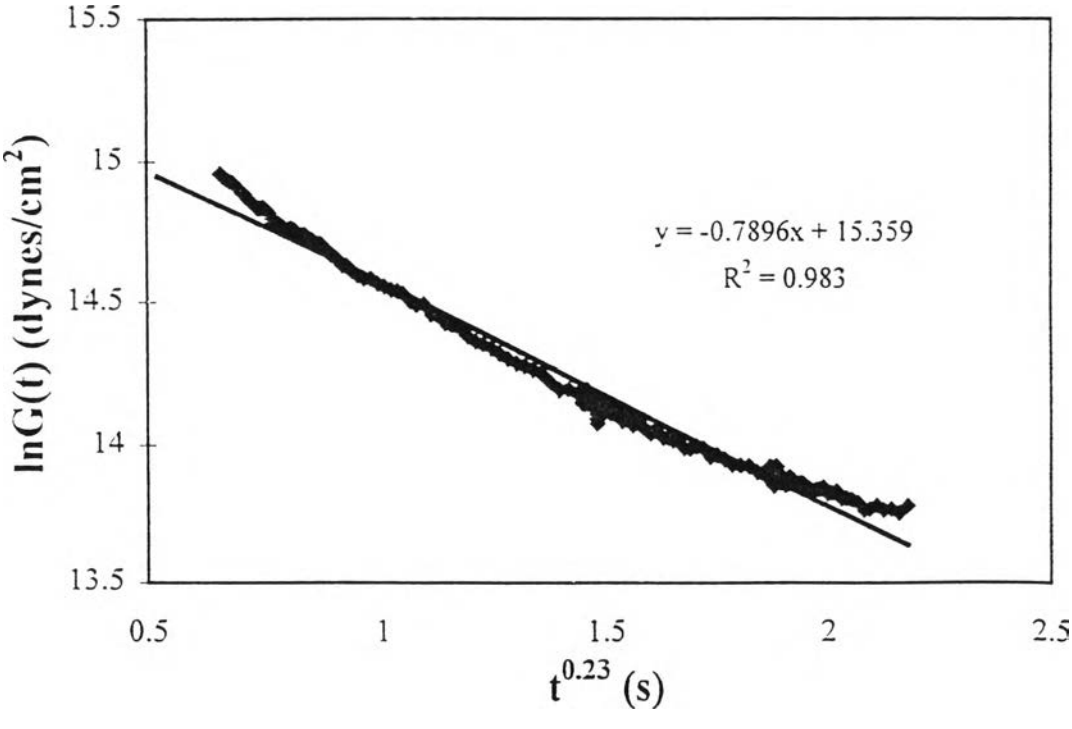

Figure 3.20 (b) The plot of $\ln G_R(t)$ vs. t^{β} of PMMA/SAN 30/70 blend at 130 °C with β of 0.23.

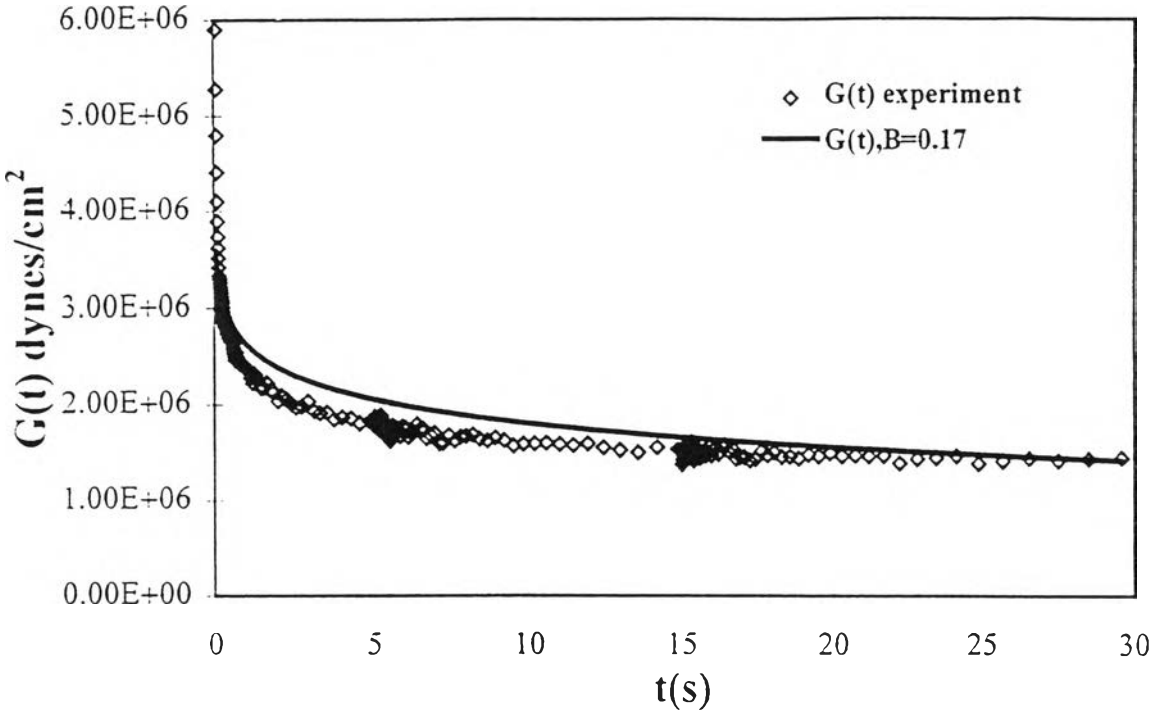

Figure 3.21 (a) Open diamonds are relaxation moduli vs. time of PMMA/SAN 30/70 blend at 60 °C with %strain of 0.3. Solid line is the theoritical stress relaxation moduli with $\beta = 0.17$.

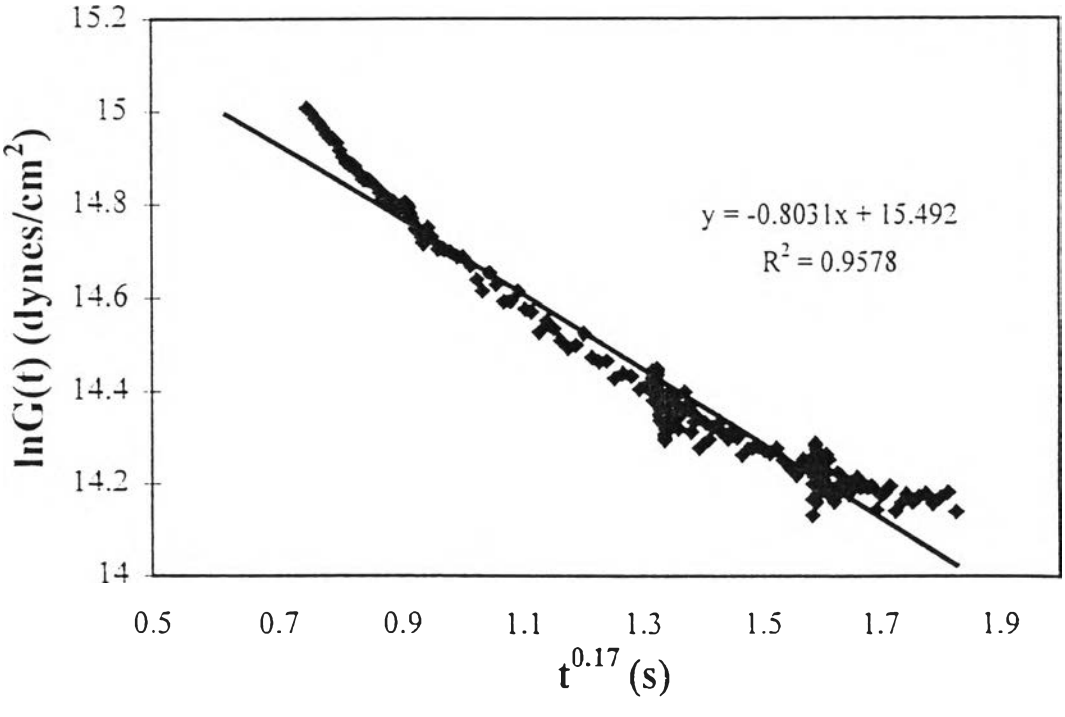

Figure 3.21 (b) The plot of $\ln G_R(t)$ vs. t^{β} of PMMA/SAN 30/70 blend at 60 °C with β of 0.17.

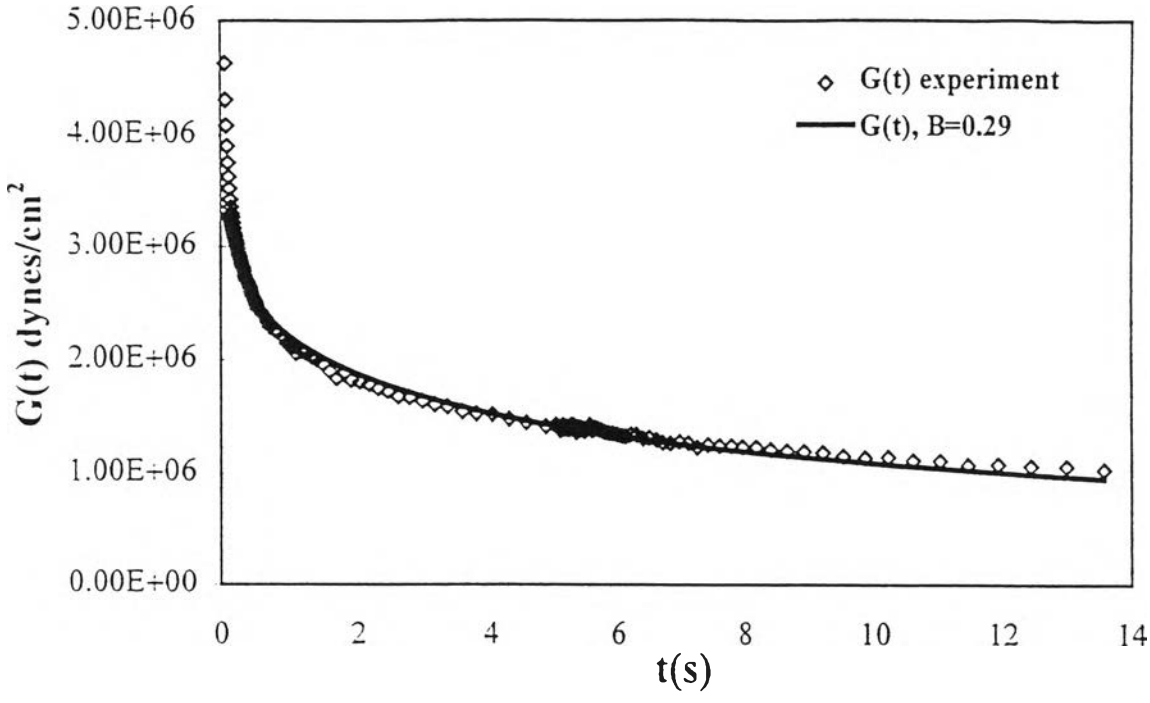

Figure 3.22 (a) Open diamonds are relaxation moduli vs. time of PMMA/SAN 30/70 blend at 80 °C with %strain of 0.3. Solid line is the theoritical stress relaxation moduli with $\beta = 0.29$.

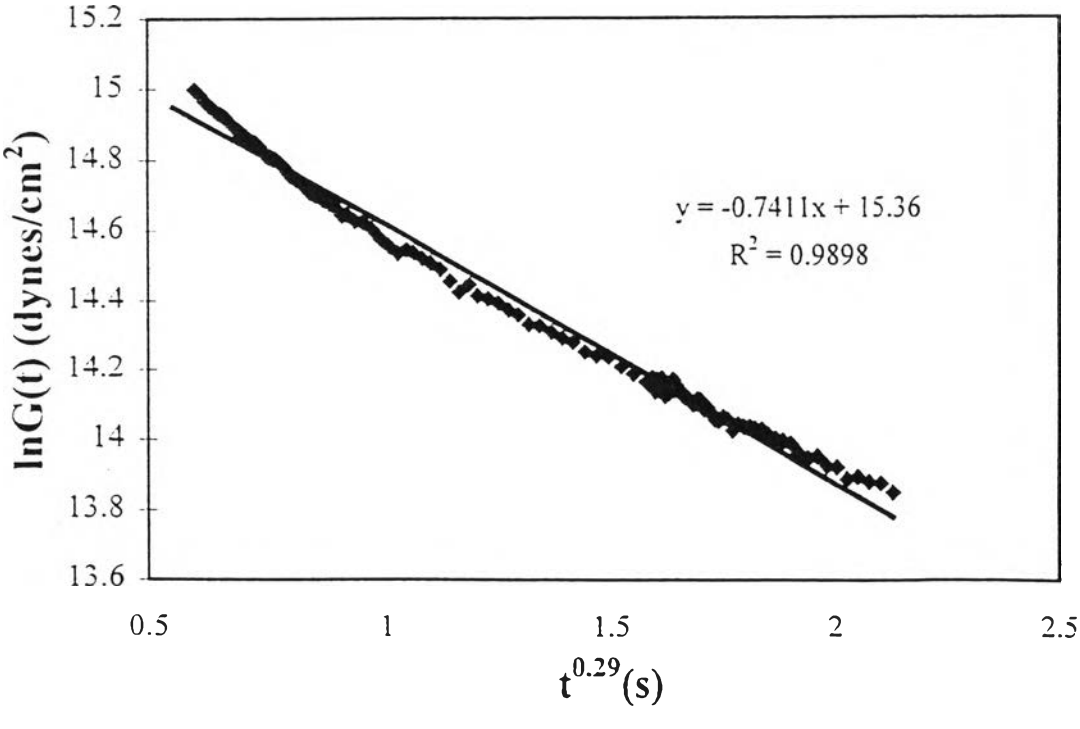

Figure 3.22 (b) The plot of $\ln G_R(t)$ vs. t^{β} of PMMA/SAN 30/70 blend at 80 °C with β of 0.29.

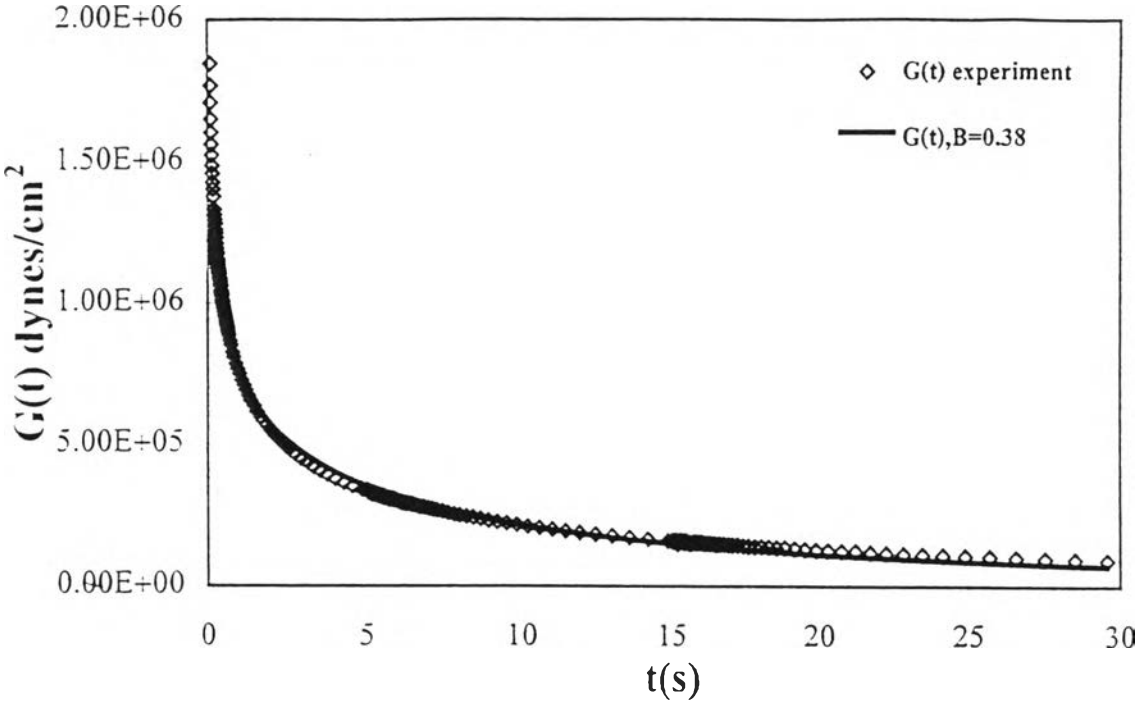

Figure 3.23 (a) Open diamonds are relaxation moduli vs. time of PMMA/SAN 30/70 blend at 150 °C with %strain of 0.3. Solid line is the theoritical stress relaxation moduli with $\beta = 0.38$.

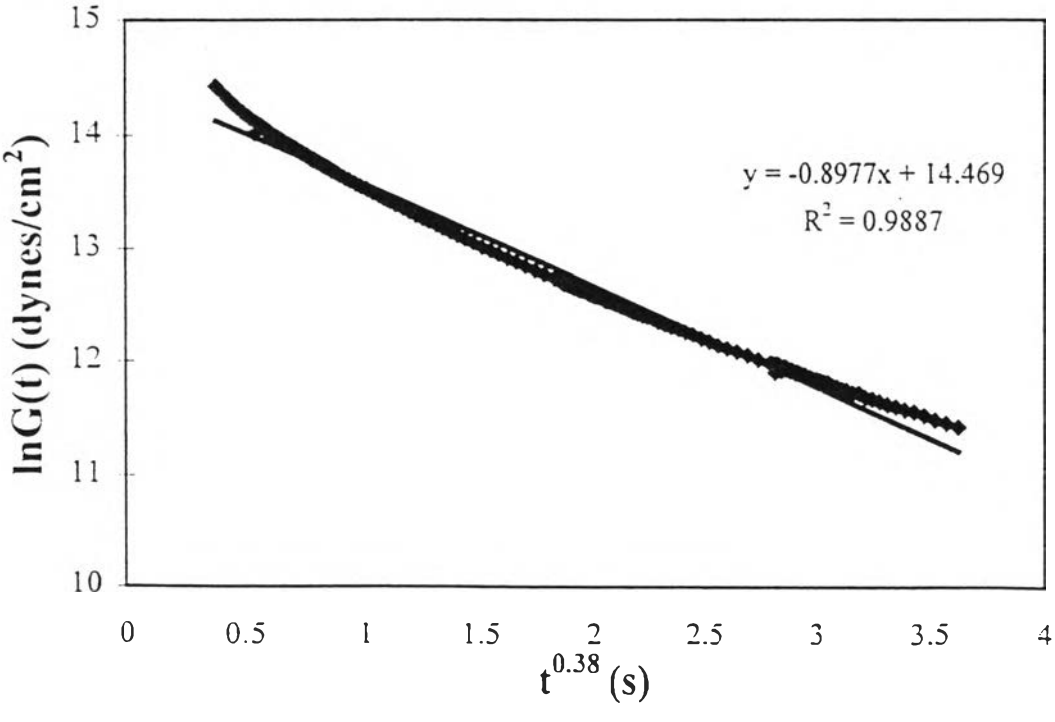

Figure 3.23 (b) The plot of $\ln G_R(t)$ vs. t^{β} of PMMA/SAN 30/70 blend at 150 °C with β of 0.38.

β and τ^* of all the samples were obtained from the best fits to our stress relaxation data. Their dependences on temperature and chemical composition are shown in Table 3.2.

Table 3.2 The coupling parameter β, and effective relaxation time τ^* at different temperatures of all the samples

Temp. (oC)	PMMA M_w = 350000		PMMA M_w = 75000		SAN		PMMA/SAN 30/70 Blend	
	β	τ^*	β	τ^*	β	τ^*	β	τ^*
180	0.41	5.65	0.4	0.27	0.35	0.14	0.32	0.15
150	0.4	17.2	0.39	0.78	0.34	0.44	0.38	1.33
130	0.36	29.5	0.39	1.01	0.38	3.1	0.23	2.79
80	0.33	0.86	0.27	0.39	0.25	2.1	0.29	2.81
70	0.17	1.28	0.27	1.96	0.17	2.12	0.2	3.48
60	0.12	697	0.15	29.6	0.25	2.14	0.17	3.63

According to the time-temperature superposition criteria [Ferry, 1980], β_η and β_α should be temperature independent. We found that the differences were small. Thus, the average values of β_η and β_α were taken and used. Averaged β_η and β_α values of all our samples are shown in Table 3.3.

Table 3.3 The averaged coupling parameter β_η and β_α of all the samples

Samples	β_η	β_α
PMMA $M_w = 350000$	0.39	0.25
PMMA $M_w = 75000$	0.39	0.27
SAN75:25	0.36	0.21
PMMA/SAN blend	0.35	0.25

Form Figures 3.17- 3.20 and Tables 3.2- 3.3, we can see that at a fixed temperature the relaxation time τ^* of both the segmental and the terminal relaxations depend on polymer structure. The coupling parameter β_η is less sensitive to polymer chemical structure whereas β_α depends strongly on polymer chemical structure. The segmental relaxation involves crowding coupling between the relaxing monomeric units. The differences in the intermolecular couplings between the different types of monomer units cause different β_α. For the terminal relaxation in entangled monodisperse polymers, the intermolecular interactions are derived from chain entanglements involving a length scale much longer the size of monomer unit. Therefore, β_η are less sensitive to polymer structure. It was stated by Alegria et al. in 1991 and Ngai et al. in 1992 that τ^* depends on degree of intermolecular interactions and should increase or decrease along with β. However, our data do not provide a conclusive evidence for this.

From Figures 3.21- 3.23 and Tables 3.2- 3.3, τ^* for both the segmental and the terminal relaxations seem to increase as temperature decreases. The different molecular processes in the softening and the terminal regimes cause differences in coupling parameter β_α and β_η. It is obvious from the Tables 3.1

and 3.2 that β_η obtained is greater than β_α for all our samples. The coupling parameter β_η, or the distribution spectrum of relaxation time, is broad due to the several molecular motions of the chains: side chain motions, segmental motions, and chain reptations. Below T_g, there is only the local segmental motions of the chains, so β_α is smaller, corresponding to a narrower distribution spectrum of relaxation time.

Alegria et al. (1991) stated that β_η in the terminal relaxation were systematically higher than β_α obtained for the α-relaxation. The differences between the coupling parameter β found for the two relaxations agree with the results reported in the literature for different kinds of polymers. Therefore our results are consistent with previous published results [Alegria et al. (1991), Ngai et al. (1992), Plazek et al. (1992), Palade et al. (1995)].

3.7.2 Shift Factors and the Coupling Model

The shift factors $(a_T)_\alpha$ were calculated by the coupling model (equation 3.2), using β_η and β_α obtained from stress relaxation measurements whereas $(a_T)_\eta$ were calculated from the WLF equation, as shown in Figures 3.24, 3.25, and 3.26.

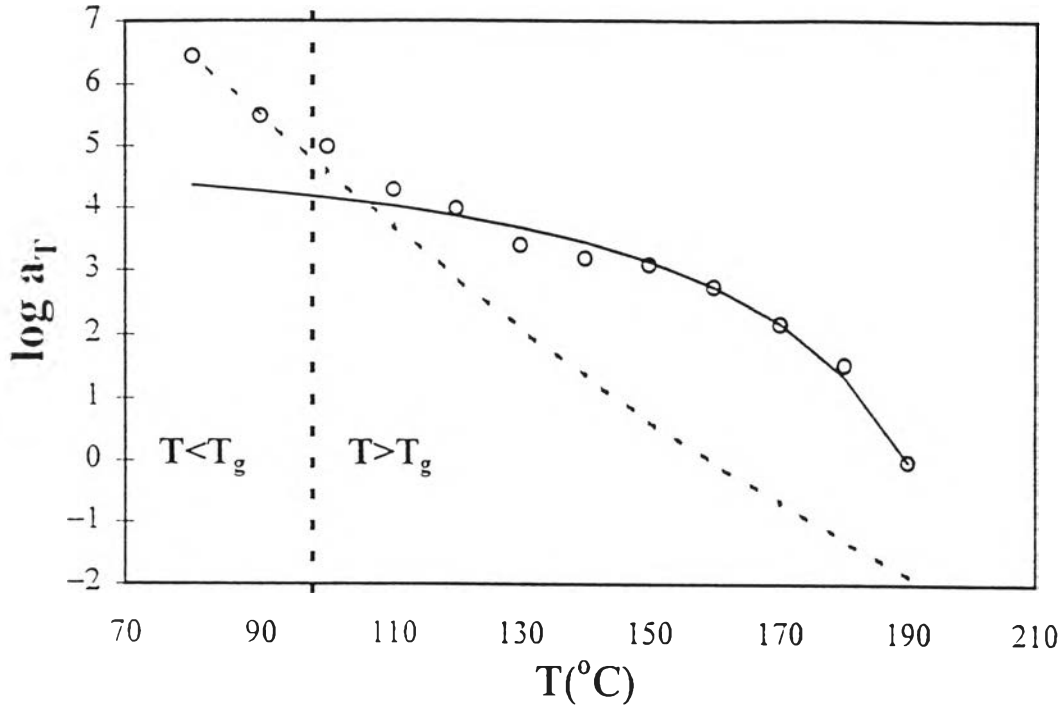

Figure 3.24 (a) Open circles are apparent shift factors of PMMA M_W = 350000 $gmol^{-1}$. Solid line is the WLF equation. Dotted line is the coupling model. The reference temperature is 190 °C.

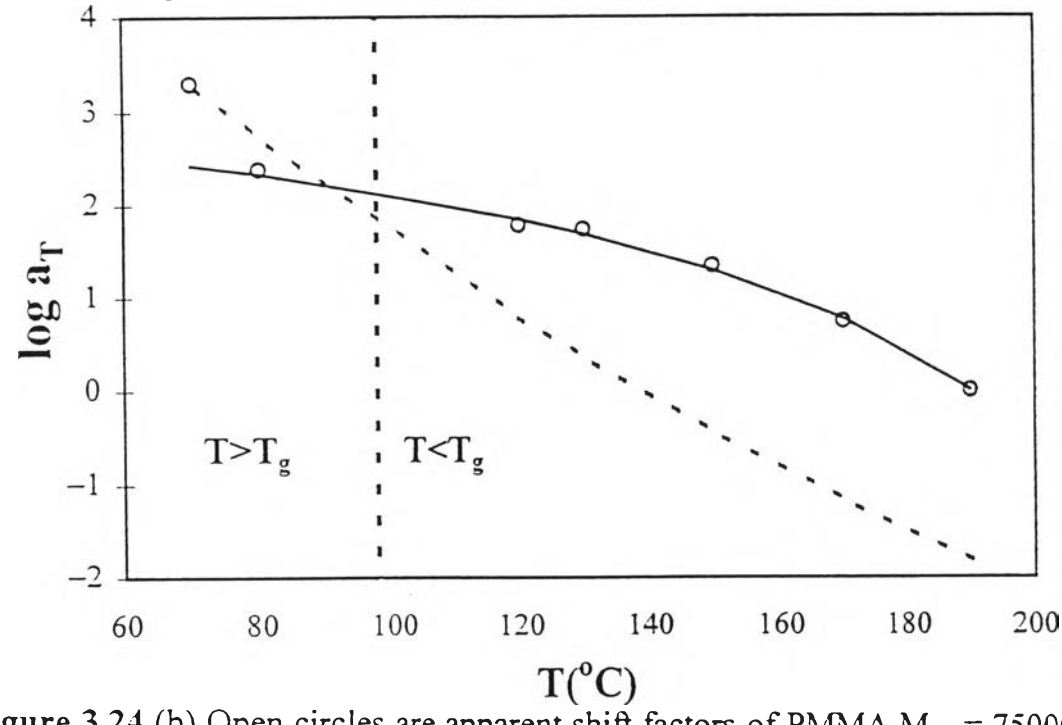

Figure 3.24 (b) Open circles are apparent shift factors of PMMA M_W = 75000 $gmol^{-1}$. Solid line is the WLF equation. Dotted line is the coupling model. The reference temperature is 190 °C.

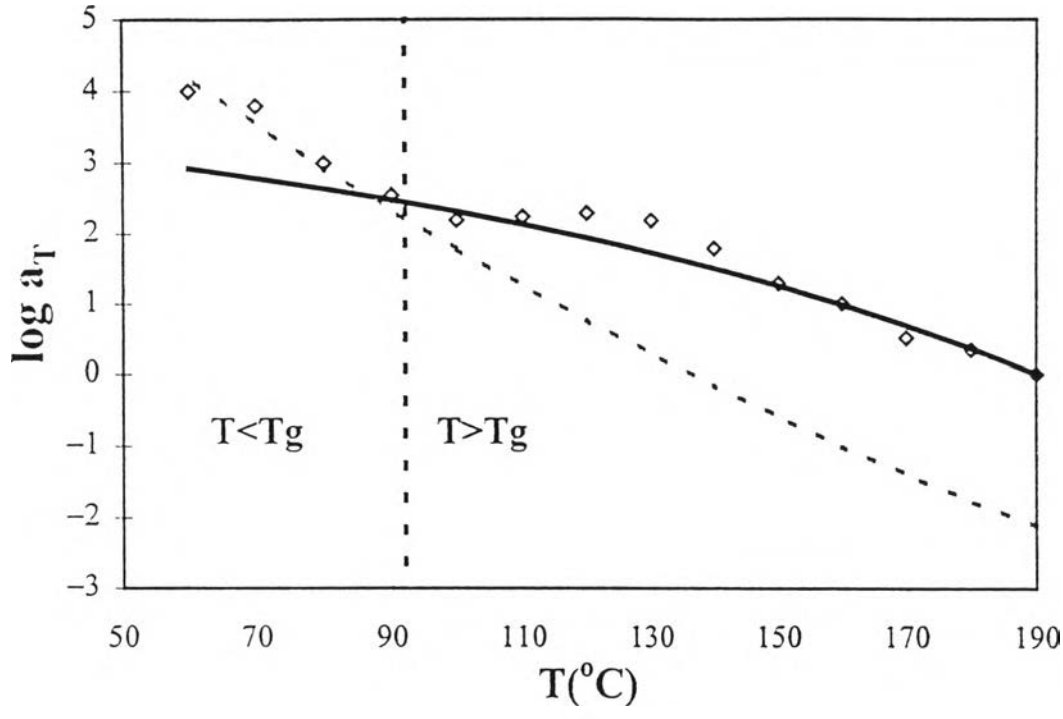

Figure 3.25 Open circles are apparent shift factors of SAN75:25. Solid line is the WLF equation. Dotted line is the coupling model. The reference temperature is 190 °C.

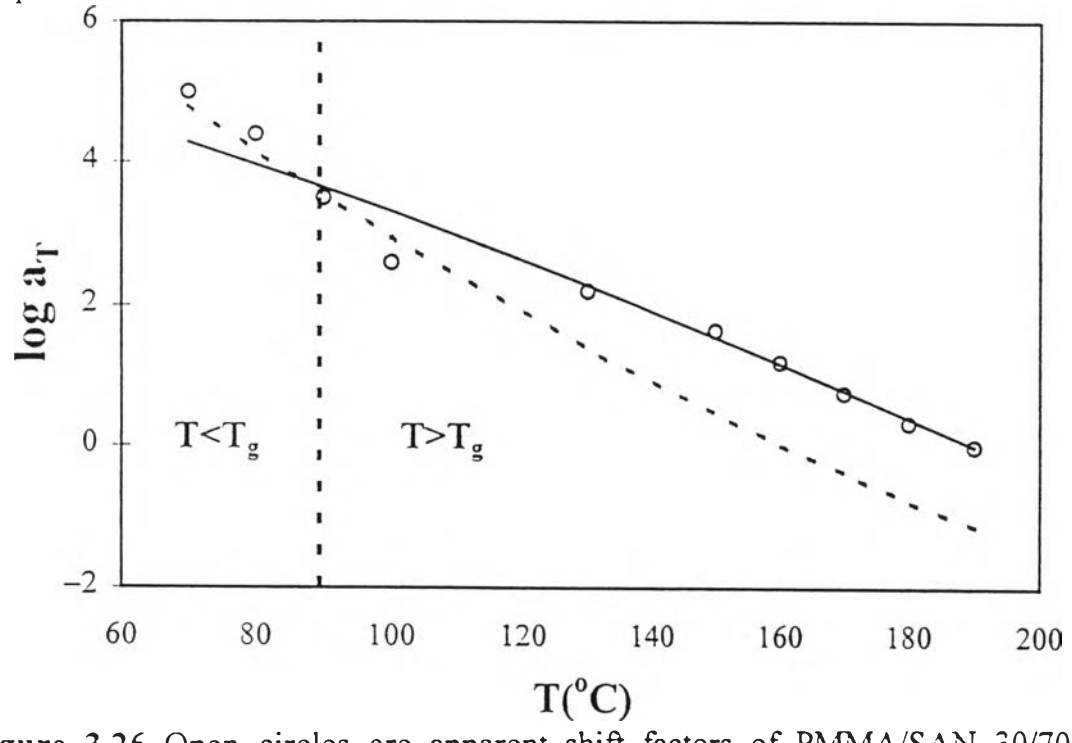

Figure 3.26 Open circles are apparent shift factors of PMMA/SAN 30/70 blend. Solid line is the WLF equation. Dotted line is the coupling model. The reference temperature is 190 °C.

Figures 3.24 to 3.26 show that the shift factors $(a_T)_\alpha$ predicted by the coupling model agree with the empirical shift factors below T_g while the extrended calculations by the WLF equation do not. Therefore, we conclude that the coupling model is successful in making a connection between the different temperature dependences of the $(a_T)_\alpha$ and $(a_T)_\eta$ in the α and the η-relaxation processes.